

Multistep oxidation of diethynyl oligophenylamine-bridged diruthenium and diiron complexes

Article

Accepted Version

Zhang, J., Guo, S.-Z., Don, Y.-B., Rao, L., Jin, Y., Yu, G.-A., Hartl, F. and Liu, S. H. (2017) Multistep oxidation of diethynyl oligophenylamine-bridged diruthenium and diiron complexes. *Inorganic Chemistry*, 56 (2). pp. 1001-1015. ISSN 0020-1669 doi: <https://doi.org/10.1021/acs.inorgchem.6b02809> Available at <https://centaur.reading.ac.uk/68545/>

It is advisable to refer to the publisher's version if you intend to cite from the work. See [Guidance on citing](#).

To link to this article DOI: <http://dx.doi.org/10.1021/acs.inorgchem.6b02809>

Publisher: American Chemical Society

All outputs in CentAUR are protected by Intellectual Property Rights law, including copyright law. Copyright and IPR is retained by the creators or other copyright holders. Terms and conditions for use of this material are defined in the [End User Agreement](#).

www.reading.ac.uk/centaur

CentAUR

Central Archive at the University of Reading

Reading's research outputs online

Multistep Oxidation of Diethynyl Oligophenylamine-Bridged Diruthenium and Diiron Complexes

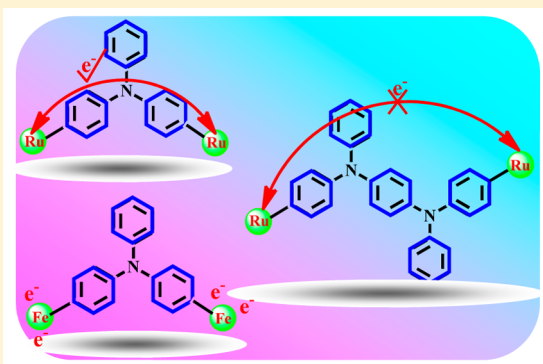
Jing Zhang,[†] Shen-Zhen Guo,[†] Yu-Bao Dong,[†] Li Rao,[†] Jun Yin,[†] Guang-Ao Yu,[†] František Hartl,^{*,‡,§} and Sheng Hua Liu^{*,†}

[†]Key Laboratory of Pesticide and Chemical Biology, Ministry of Education, College of Chemistry, Central China Normal University, Wuhan 430079, P. R. China

[‡]Department of Chemistry, University of Reading, Whiteknights, Reading RG6 6AD, U.K.

[§] Supporting Information

ABSTRACT: Homo-dinuclear nonlinear complexes $[\{M(dppe)-Cp^*\}_2\{\mu-(C\equiv C)_2X\}]$ ($dppe = 1,2$ -bis(diphenylphosphino)ethane; $Cp^* = \eta^5-C_5Me_5$; $X =$ triphenylamine (TPA), $M = Ru$ (**1a**) and Fe (**1b**); $X = N,N,N',N'$ -tetraphenylphenylene-1,4-diamine (TPPD), $M = Ru$ (**2a**)) were prepared and characterized by 1H , ^{13}C , and ^{31}P NMR spectroscopy and single-crystal X-ray diffraction (**1a**, **2a**). Attempts to prepare the di-iron analogue of **2a** were not successful. Experimental data obtained from cyclic voltammetry, square wave voltammetry, UV–vis–NIR (NIR = near-infrared) spectro-electrochemistry, and very informative IR spectro-electrochemistry in the $C\equiv C$ stretching region, combined with density functional theory calculations, afford to make an emphasizing assessment of the close association between the metal–ethynyl termini and the oligophenylamine bridge core as well as their respective involvement in sequential one-electron oxidations of these complexes. The anodic behavior of the homo-bimetallic complexes depends strongly both on the metal center and the length of the oligophenylamine bridge core. The poorly separated first two oxidations of di-iron complex **1b** are localized on the electronically nearly independent Fe termini. In contrast, diruthenium complex **1a** exhibits a significantly delocalized character and a marked electronic communication between the ruthenium centers through the diethynyl–TPA bridge. The ruthenium–ethynyl halves in **2a**, separated by the doubly extended and more flexible TPPD bridge core, show a lower degree of electronic coupling, resulting in close-lying first two anodic waves and the NIR electronic absorption of $[2a]^+$ with an indistinctive intervalence charge transfer character. Finally, the third anodic waves in the voltammetric responses of the homo-bimetallic complexes are associated with the concurrent exclusive oxidation of the TPA or TPPD bridge cores.



INTRODUCTION

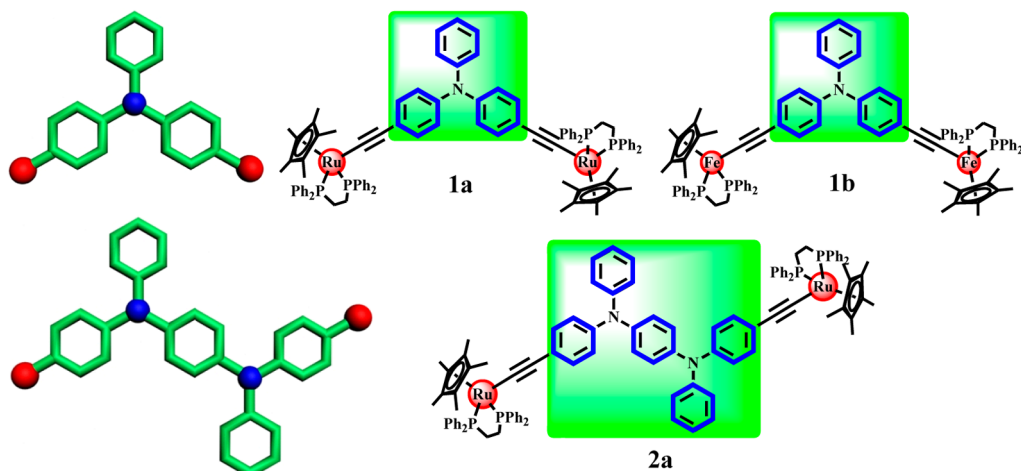
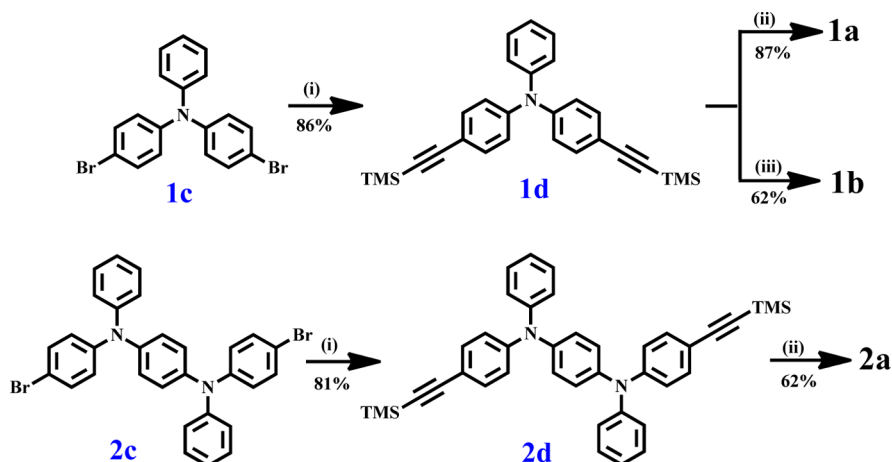
In recent years mixed-valence (MV) states of binuclear complexes have attracted considerable attention,^{1,2} providing important model systems for intramolecular charge transfer processes and offering broad prospects for building highly functionalized molecules with interesting electronic and optoelectronic properties essential for molecular scale electroactive materials and devices.^{3–6} In this respect, numerous studies focused in the past decades on rigid and π -conjugated bridging ligands connecting two redox-active metallic termini, as the simplest models for the electron-transfer phenomena in the MV systems.^{7–10} Comprehensive studies have explored a wide range of systems designed to provide some insight into electron transfer over a long distance.¹¹ However, increasing the chain length to a modest degree decreased significantly solubility of the prototypical π -conjugated systems in common organic solvents, and the complexity of their syntheses essentially arose. These factors present obstacles for the relevant fundamental research and restrict the longitudinal extension and processability in electronic devices.¹¹ In this

respect, continued search for novel or modified perspective systems to eliminate the above-mentioned drawbacks is very meaningful and challenging.

Triphenylamine (TPA) and other mono- and oligomeric triarylamine derivatives have widely been used as selective one-electron reductants, electrocatalysts, and hole-transporting materials in organic optoelectronic devices, such as photoconductors, photorefractive materials, and organic light-emitting devices. This is ascribed to their favorable redox properties, with one or more readily accessible oxidations and high stabilities of the corresponding radical cations with appropriate substitution patterns.^{12–14} Moreover, TPA has also been considered as an ideal redox center to study the intermolecular electron transfer processes in MV systems.^{15–17} Despite the efforts, reports on mixed-valence systems featuring the TPA unit as (a component of) a bridging ligand are relatively limited in number compared with the π -conjugated

Received: November 23, 2016

Chart 1. Studied Diethynyl Oligophenylamine-Bridged Homo-Bimetallic Ruthenium and Iron Complexes

Scheme 1. General Synthetic Routes to Complexes 1a, 1b, and 2a^a

^aReagents and conditions: (i) $[\text{Pd}(\text{PPh}_3)_4]$, CuI, Et_3N , TMSA, in THF; (ii) $[\text{RuCl}(\text{dppe})\text{Cp}^*]$, KF, MeOH/THF; (iii) K_2CO_3 in CH_3OH , $[\text{FeCl}(\text{dppe})\text{Cp}^*]$, NaBPh_4 , *t*-BuOK.

systems,¹⁸ let alone a detailed discussion of their electronic properties.^{18d} In another aspect, a nonrigid TPA-based structure with appropriate substituents^{12–14} offers a viable solution to the problem of poorly soluble elongated systems and the difficulty in synthesizing large dendrimers. Notably, Onitsuka and co-workers synthesized successfully a series of ruthenium–acetylide dendrimers with the tris(4-ethynylphenyl)amine bridging ligand up to the second generation by using a convergent method.¹⁸ⁱ In this work we focus on TPA and scarcely reported tetraphenylphenylenediamine (TPPD) in the core of the diethynyl-terminated bridge. The external “ $\text{Ru}(\text{dppe})\text{Cp}^*$ ” and “ $\text{Fe}(\text{dppe})\text{Cp}^*$ ” (dppe = 1,2-bis(diphenylphosphino)ethane; Cp^* = $\eta^5\text{-C}_5\text{Me}_5$) units completing the studied homo-bimetallic chains (Chart 1) are particularly suited as reference redox-active termini in molecular wire models to study their MV properties, as documented by the previously reported work.^{2d–h,19} The assembly of multiple redox-active components was anticipated to exhibit peculiar electrochemical and photophysical properties. Hereinafter we detail our efforts to explore to which degree the redox, spectroscopic, and bonding properties and electronic communication in the investigated homo-bimetallic series are affected by the varied combination of the oligophenylamine

bridge core and the metal centers. The input data for the discussion have been obtained by using controlled-potential voltammetry and UV–vis–NIR/IR (NIR = near-infrared) spectro-electrochemistry combined with density functional theory (DFT) calculations.

RESULTS AND DISCUSSION

Syntheses and Characterization. The general synthetic route to homo-dinuclear metal complexes **1a**, **1b**, and **2a** is outlined in Scheme 1. Bridge precursors **1d** and **2d** were obtained in yields higher than 80%, having used Pd/Cu-catalyzed Sonogashira coupling reactions between 4-bromo-*N*-(4-bromophenyl)-*N*-phenylaniline (**1c**), *N*¹,*N*⁴-bis(4-bromophenyl)-*N*¹,*N*⁴-diphenylbenzene-1,4-diamine (**2c**), and trimethylsilylacetylene (TMSA), respectively. Subsequently, the trimethylsilyl (TMS) termini in compounds **1d** and **2d** were deprotected with KF or K_2CO_3 to give the terminal bis(alkyne) and then reacted with $[\text{RuCl}(\text{dppe})\text{Cp}^*]$ and $[\text{FeCl}(\text{dppe})\text{Cp}^*]$ to obtain the corresponding target complexes **1a**, **2a**, and **1b**, respectively. Unfortunately, deprotected **2d** did not coordinate to the $\text{Fe}(\text{dppe})\text{Cp}^*$ termini by this procedure,²⁰ and the intended diethynyl-TPPD diiron complex (**2b**) was not obtained. Notably, no obvious differences have been observed

in comparative NMR responses of related diruthenium complexes **1a** and **2a**, specifically, the dppe signals in the ^1H and ^{31}P NMR spectra and the $\text{Ru}-\text{C}\equiv\text{C}$ signals in the ^{13}C NMR spectra.

X-ray Crystallography. The molecular structures of solid **1a** and **2a** were resolved by single-crystal X-ray diffraction. Pertinent diffraction parameters are given in Table S1 (see the Supporting Information). Important bond lengths (Å), bond angles (deg), and $\text{Ru}\cdots\text{Ru}$ distances (Å) in the crystal structures are collected in Table 1. The structures of **1a** and **2a** feature

Table 1. Selected Bond Lengths (Å), Angles (deg), and Inter-Ruthenium Distances (Å) in the Crystal Structures of Complexes **1a** and **2a**

complex 1a			
Ru(1)–C(37)	1.999 (3)	C(43)–C(44)	1.378 (4)
Ru(1)–P(1,2)	2.250 (9), 2.258 (8)	C(39)–C(44)	1.395 (5)
C(37)–C(38)	1.209 (4)	C(45)–C(46)	1.384 (4)
C(38)–C(39)	1.436 (4)	C(46)–C(47)	1.378 (5)
C(39)–C(40)	1.401 (5)	C(47)–C(48)	1.371 (5)
C(40)–C(41)	1.382 (4)	N(1)–C(42)	1.426 (3)
C(41)–C(42)	1.387 (4)	N(1)–C(45)	1.403 (5)
C(42)–C(43)	1.391 (4)	Ru(1)···Ru(2)	14.19
P(1)–Ru(1)–P(2)	83.3 (3)		
Ru(1)–C(37)–C(38)	174.9 (3)		
C(37)–C(38)–C(39)	175.6 (3)		
complex 2a			
Ru(1)–C(27)	1.991 (5)	C(36)–C(37)	1.343 (2)
Ru(1)–P(1,2)	2.246 (3), 2.248 (3)	C(37)–C(38)	1.390 (2)
C(27)–C(28)	1.214 (9)	C(38)–C(39)	1.394 (2)
C(28)–C(29)	1.448 (7)	C(39)–C(40)	1.348 (2)
C(29)–C(30)	1.375 (9)	C(35)–C(40)	1.402 (8)
C(30)–C(31)	1.360 (8)	C(41)–C(42)	1.363 (9)
C(31)–C(32)	1.390 (9)	C(42)–C(43)	1.393 (9)
C(32)–C(33)	1.378 (9)	C(41)–C(43)	1.390 (8)
C(33)–C(34)	1.389 (7)	N(1)–C(32)	1.428 (5)
C(29)–C(34)	1.392 (2)	N(1)–C(41)	1.424 (6)
C(35)–C(36)	1.392 (2)	Ru(1)···Ru(2)	20.68
P(1)–Ru(1)–P(2)	84.4 (3)		
Ru(1)–C(37)–C(38)	178.5 (3)		
C(37)–C(38)–C(39)	176.1 (3)		

approximately linear $\text{Ru}-\text{C}\equiv\text{C}-\text{C}$ moieties, the pairs of $\text{Ru}-\text{C}\equiv\text{C}$ and $\text{C}\equiv\text{C}-\text{C}$ angles being 174.9° , 175.6° and 178.5° , 176.1° , respectively. As seen in Figure 1 and Figure S1(A) (Supporting Information), the crystallographic analysis manifests typical pseudo-octahedral geometry around the ruthenium centers. The $\text{C}\equiv\text{C}$ bond lengths [1.209 Å (**1a**) and 1.214 Å (**2a**)] comply with a carbon–carbon triple bond, and the bonding parameters of the $\text{Ru}(\text{dppe})\text{Cp}^*$ group, including the $\text{Ru}-\text{C}$ and $\text{Ru}-\text{P}$ distances and $\text{P}-\text{Ru}-\text{P}$ angles, compare well with the data reported for a range of similar systems.^{21,22} Elongation of the bridging ligand core from monoamine (TPA) in **1a** to diamine (TPPD) in **2a** caused the $\text{Ru}(1)\cdots\text{Ru}(2)$ distance to increase considerably from 14.19 to 20.68 Å . These data are consistent with the corresponding calculated results presented hereinafter.

Some additional interesting features can be found in the crystal packing (Figure S1(B)). Complex **2a** shows typical lamellar packing characteristics with the parallel arrangements of the bridge and metallic termini in each layer from the side view of the lamellar structure, the benzene rings 1, 3 and 2, 4 of the diamine bridge core (Figure S1(B)) being oriented in opposite directions and arranged in parallel with each other.

Electrochemical Properties. The anodic behavior of complexes **1a**, **1b**, and **2a** was investigated by cyclic voltammetry (CV) and square-wave voltammetry (SWV) in deaerated dichloromethane containing $1 \times 10^{-1}\text{ M}$ $n\text{-Bu}_4\text{NPF}_6$ as the supporting electrolyte (Figure 2). The TMS-terminated precursors **1d** and **2d** (Scheme 1) were also studied for comparison (see Supporting Information, Figure S2). The relevant electrochemical data are summarized in Table 2.

Complexes **1a** and **1b** exhibit three successive oxidation steps. The anodic behavior of **2a** is more complex, and only the first four anodic processes were investigated. Comparing the electrochemical behavior of diruthenium complexes **1a** and **2a**, the potentials of their first three anodic steps ($E_{1/2}(1,2,3)$) are similar. The main difference arises in the wave splitting $\Delta E_{1/2}(1-2)$ and the thermodynamic stability (comproportionation) constant K_c of $[\mathbf{2a}]^+$, which is considerably smaller than that determined for $[\mathbf{1a}]^+$ (Table 2). This result has likely its origin in the extended bridge core in **2a** and limited electronic communication between two redox active $\text{Ru}-\text{C}\equiv\text{C}$ units, resembling in this respect an earlier reported series of

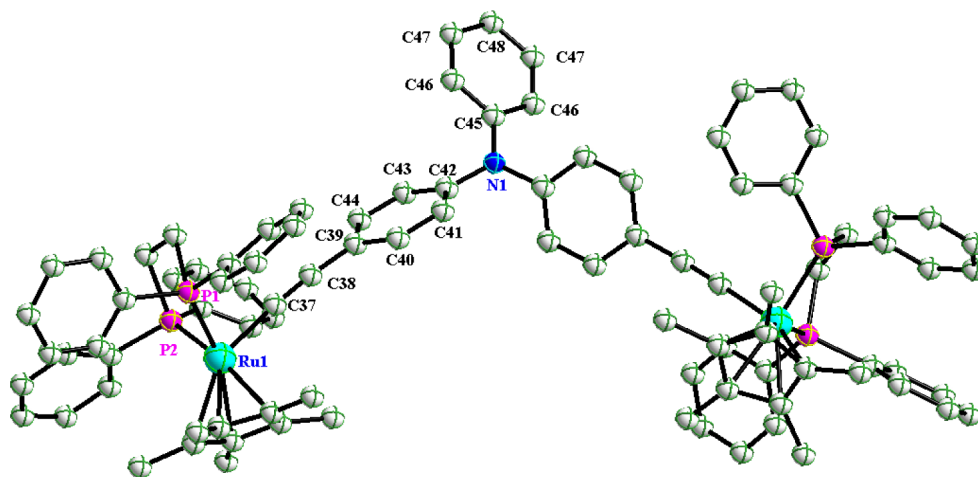


Figure 1. X-ray crystal structure of **1a** shown with thermal ellipsoids at the 50% probability level. Hydrogen atoms were omitted for clarity. Full crystallographic details are given in Supporting Information. CCDC No. 1435472.

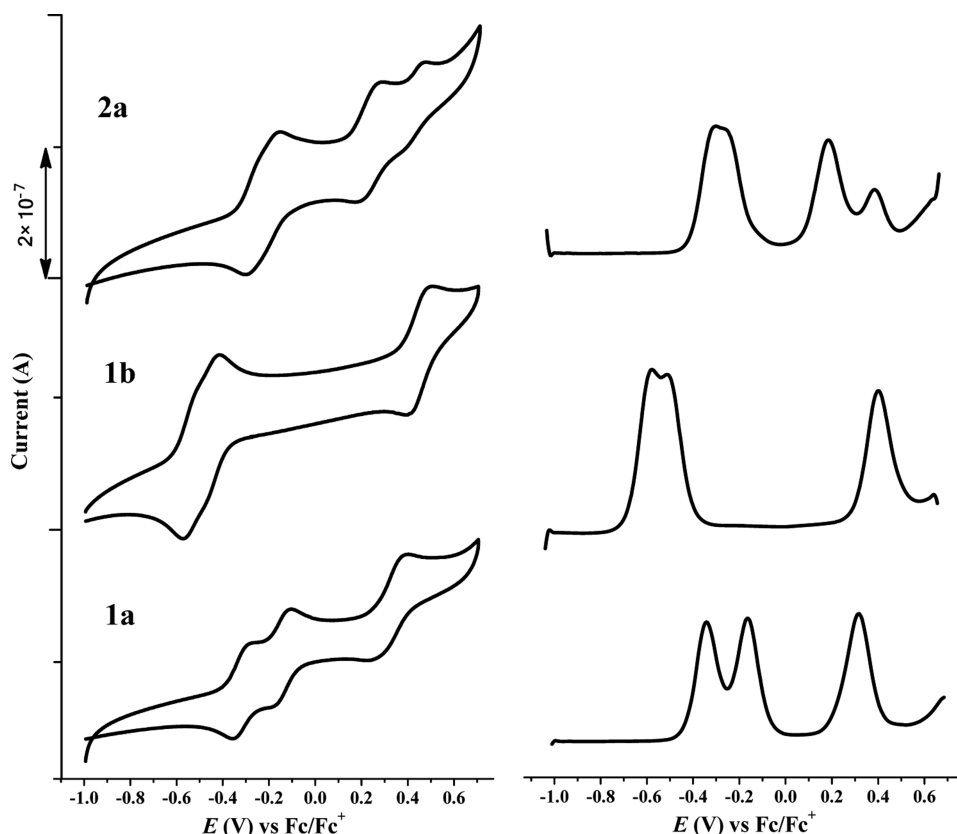


Figure 2. (left) CV of complexes **1a**, **1b**, and **2a** in $\text{CH}_2\text{Cl}_2/n\text{-Bu}_4\text{NPF}_6$ at $\nu = 50 \text{ mV s}^{-1}$. (right) Corresponding SWV of complexes **1a**, **1b**, and **2a** at $f = 10 \text{ Hz}$ and $t_p = 25 \text{ mV}$.

Table 2. Electrochemical Data for Complexes 1a, 1b, and 2a, TMS-Terminated Reference Compounds 1d and 2d, a Dinuclear Vinyl–Ruthenium Complex Related to 1a, and Reference Phenylamines^a

compound	$E_{1/2}(1) \text{ (V)}$	$E_{1/2}(2) \text{ (V)}$	$E_{1/2}(3) \text{ (V)}$	$E_{1/2}(4) \text{ (V)}$	$\Delta E_{1/2}(1-2) \text{ (mV)}$	K_c^b
1a	−0.36	−0.18	0.30		180	1.1×10^3
Ru–vinyl^c	−0.17	0.15	0.59		320	3.8×10^5
1b	−0.56	−0.50	0.41		60	10
1d	0.66					
TPA^d	0.70 ^{e,f}					
2a	−0.31	−0.26	0.19	0.39	50	7
2d	0.21	0.68				
TPPD^d	0.14 ^f	0.63				

^aThe anodic potentials are referenced against the standard ferrocene/ferrocenium (Fc/Fc^+) redox couple. ^bThe comproportionation constants K_c were estimated using the expression $K_c = \exp(\Delta E/25.69 \text{ mV})$ at 298 K, with input data recorded at $\nu = 50 \text{ mV s}^{-1}$. ^c $[\{\text{Cl}(\text{CO})(\text{P}(\text{t}\text{Bu})\text{R}_3)_2\text{Ru}-\text{CH}=\text{CH}-\text{C}_6\text{H}_4-\}_2\text{N}-\text{C}_6\text{H}_4\text{OCH}_3]$. ^dReference 18f. ^eIrreversible anodic peak potential. ^fPotential determined against an Ag/AgCl reference electrode; $E_{1/2}(\text{Fc}/\text{Fc}^+) = +0.43 \text{ V}$ versus Ag/AgCl .

oligothiophene-bridged diruthenium diethynyl complexes.²¹ The additional fourth anodic wave of **2a** at a higher potential can safely be ascribed to the second oxidation of the diamine core, based on comparison with the anodic potentials of the TMS-terminated diethynyl TPPD reference compound **2d**. The obvious difference in the composition of **1a** and **1b** is the metallic redox center. Interestingly, the replacement of ruthenium in **1a** with iron in **1b** resulted in a slightly negative shift of the first anodic wave (at $E_{1/2}(1)$) and significantly decreased comproportionation constant K_c (Table 2). It will be shown in the spectro-electrochemical section that the formally Fe(II) centers in the terminal positions of **1b** oxidize in a more localized fashion compared to the Ru(II) derivative, **1a**, as also encountered in the literature for related compounds.^{3c,8b,18h,23}

Accordingly, the two formally Fe(II) centers in **1b** communicate poorly through the twisted ethynyl–phenylene–N–phenylene–ethynyl bridge, in line with the small $\Delta E_{1/2}(1-2)$ and K_c values for **[1b]⁺**. Consequently, it was hardly possible to record IR and UV–vis–NIR spectra of “pure” **[1b]⁺** in the course of the corresponding spectro-electrochemical experiments described in the following section. A less severe restriction applies in this regard for **[2a]⁺**.

A significantly greater involvement of the TPA core in the electrochemical oxidation has been reported^{18d} for a bridged dinuclear vinyl–ruthenium complex, causing a stronger electronic interaction between the ruthenium–vinyl linker subunits in the corresponding one-electron oxidized cation and a larger K_c value (Table 2). The different auxiliary ligands at the

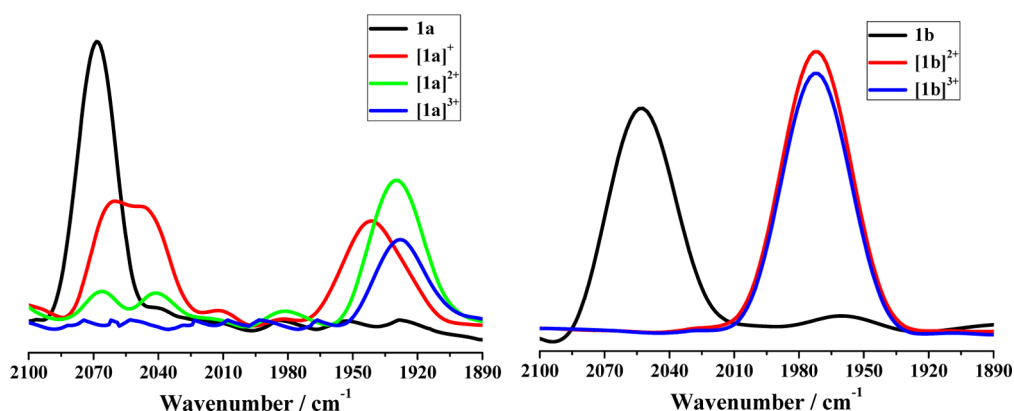


Figure 3. IR spectra recorded in the $\nu(\text{C}\equiv\text{C})$ region for complexes **1a** and **1b** in different oxidation states generated in $\text{CH}_2\text{Cl}_2/1 \times 10^{-1} \text{ M } n\text{-Bu}_4\text{NPF}_6$ at 298 K within an OTTLE cell. For the chemical oxidation of **1b** to $[\mathbf{1b}]^+$ see [Supporting Information](#), Figure S6.

193 ruthenium center, specifically, *trans*- $\text{RuCl}(\text{CO})\{\text{P}(i\text{-Pr})_3\}_2$, also
194 play a role in the control of the electronic conjugation between
195 the TPA bridge core and the ruthenium–linker (vinyl vs
196 ethynyl) subunits. For example, smaller differences in the
197 anodic behavior exist between TPA-based mono- and trinuclear
198 vinyl–ruthenium^{18d} and ethynyl–ruthenium²⁴ complexes with
199 similar ruthenium coordination sites.

200 **IR and UV–vis–NIR Spectro-Electrochemistry.** IR and
201 UV–vis–NIR spectro-electrochemical studies were undertaken
202 to get insight into the nature of the physical and electronic
203 structures in different oxidation states within the investigated
204 three redox series.

205 The IR spectra of neutral complexes **1a**, **1b**, and **2a** are
206 characterized by a strong single $\nu(\text{C}\equiv\text{C})$ band ([Figure 3](#),
207 [Figure S3](#) ([Supporting Information](#)), and [Table 3](#)). By contrast,

individual ethynyl–ruthenium moieties in the oxidation
217 process.

218 The second anodic step toward $[\mathbf{1a}]^{2+}$ led to the
219 disappearance of both $\nu(\text{C}\equiv\text{C})$ bands close to the wave-
220 number of the neutral parent state, while a new single band at
221 1930 cm^{-1} gained intensity. This behavior suggests the
222 complete oxidation of both $\text{Ru}-\text{C}\equiv\text{C}$ centers in $[\mathbf{1a}]^{2+}$.
223 Importantly, no prominent low-energy shift of the $\nu(\text{C}\equiv\text{C})$
224 mode was observed for the subsequent anodic generation of the
225 tricationic product $[\mathbf{1a}]^{3+}$, characterized by a single absorption
226 band marking a symmetric electronic structure. The very little
227 $\nu(\text{C}\equiv\text{C})$ shift compares well with the invariable $\nu(\text{C}\equiv\text{C})$
228 wavenumber encountered for the TMS-terminated diethynyl
229 TPA reference **1d** and its monocation ([Supporting](#)
230 [Information](#), [Figure S4](#)), suggesting the dominantly TPA-
231 localized one-electron oxidation of $[\mathbf{1a}]^{2+}$.
232

233 The anodic conversion of **2a** to $[\mathbf{2a}]^{2+}$ was marked by
234 gradual disappearance of the parent $\nu(\text{C}\equiv\text{C})$ absorption at
235 2068 cm^{-1} and the growth of a new absorption band at 1934
236 cm^{-1} belonging to the dication ([Supporting Information](#),
237 [Figure S3](#)). The red shift of 134 cm^{-1} is close to that of 138
238 cm^{-1} observed for the oxidation of **1a** to $[\mathbf{1a}]^{2+}$ ([Table 3](#)),
239 indicating comparable participation of the ethynyl linkers in the
240 oxidation of **2a** to the symmetric dication, in line with the
241 theoretical description (see below). The small separation of the
242 first two anodic waves of **2a** implies that singly oxidized $[\mathbf{2a}]^+$
243 can hardly be observed in the pure form. The IR spectrum in
244 [Figure S3](#) corresponding to the redox equilibrium with the
245 highest concentration of $[\mathbf{2a}]^+$ was selected with the aid of the
246 characteristic NIR electronic absorption of the monocation (see
247 below) simultaneously monitored in the course of the careful
248 anodic electrolysis within the OTTLE cell. It can safely be
249 concluded that $[\mathbf{2a}]^+$ exists only in a single conformation
250 detectable on the time scale inherent to IR spectroscopy,
251 differently from $[\mathbf{1a}]^+$ (see above). The IR $\nu(\text{C}\equiv\text{C})$
252 absorption of $[\mathbf{2a}]^+$ overlaps with those of parent **2a** and
253 ultimately $[\mathbf{2a}]^{2+}$ ([Table 3](#)), rendering the monocation with
254 weak electronic coupling between the $\text{Ru}-\text{C}\equiv\text{C}$ termini not
255 exceeding that in $[\mathbf{1a}]^+$, in line with the corresponding CV
256 responses ([Table 2](#)).

257 The third anodic step producing stable $[\mathbf{2a}]^{3+}$ was not
258 accompanied by any $\nu(\text{C}\equiv\text{C})$ shift, causing merely a strongly
259 diminished intensity of the $\nu(\text{C}\equiv\text{C})$ band at 1934 cm^{-1}
260 ([Figure S3](#)). This behavior reflects the dominant oxidation of
261 the TPPD bridge core in $[\mathbf{2a}]^{2+}$ to the corresponding radical
262 cation. This assignment is supported by the invariable $\nu(\text{C}\equiv\text{C})$

Table 3. Spectro-Electrochemically Determined $\nu(\text{C}\equiv\text{C})$ Wavenumbers (cm^{-1}) for $[\mathbf{1a}]^{n+}$, $[\mathbf{1b}]^{n+}$, $[\mathbf{1d}]^{n+}$ and $[\mathbf{2a}]^{n+}$, $[\mathbf{2d}]^{n+}$

complex	$n = 0$	$n = 1$	$n = 2$	$n = 3$	$n = 4$
$[\mathbf{1a}]^{n+}$	2068 (s)	2059 (m), 2046 (m), 1941 (m)	1930 (m)	1928 (w- m)	
$[\mathbf{1b}]^{n+}$	2052 (s)	^a	1972 (s)	1972 (s)	
$[\mathbf{1d}]^{n+}$	2065	2065			
$[\mathbf{2a}]^{n+}$	2068 (s)	2066, 1935 ^b	1934 (s)	1933 (w)	^c
$[\mathbf{2d}]^{n+}$	2066 (m)	2066 (m)	2066 (s)		

^aThe $\nu(\text{C}\equiv\text{C})$ absorption of $[\mathbf{1b}]^+$ is not reported due to the small K_c value and a low conversion evidenced by UV–vis–NIR spectroscopy ([Supporting Information](#), [Figure S6](#)). ^bThis absorption does not correspond to the pure form of $[\mathbf{2a}]^+$ due to small K_c but to the maximum conversion reached by electrochemical oxidation of **2a** determined by parallel UV–vis–NIR monitoring ([Supporting Information](#), [Figure S12](#)). ^cNo $\nu(\text{C}\equiv\text{C})$ band perceptible.

208 the $\nu(\text{C}\equiv\text{C})$ pattern of one-electron-oxidized $[\mathbf{1a}]^+$ is more
209 complex, consisting of a strongly shifted, fairly broad, and
210 slightly asymmetric absorption band at 1941 cm^{-1} and two
211 overlapping $\nu(\text{C}\equiv\text{C})$ bands at 2059 and 2046 cm^{-1} , that is,
212 near the absorption of parent **1a** at 2068 cm^{-1} . These spectral
213 changes comply with the presence of a symmetry-broken
214 radical cation $[\mathbf{1a}]^+$ on the time scale of IR spectroscopy ($1 \times$
215 10^{-11} to $1 \times 10^{-12} \text{ s}$), existing in different conformations
216 (rotamers)²⁵ with slightly different participation of the

wavenumber in the TMS-terminated reference redox series $[2d]^{n+}$ ($n = 0, 1, 2$); see Table 3 and Supporting Information, Figure S4.

The poorly resolved first two anodic steps of **1b** (Table 2 and Figure 2) resemble the oxidation of **2a**. We note that the $\nu(\text{C}\equiv\text{C})$ shift induced by the oxidation of **1b** to $[1b]^{2+}$ is merely 80 cm^{-1} compared to 134 cm^{-1} for $2a \rightarrow [2a]^{2+}$, and 138 cm^{-1} for $1a \rightarrow [1a]^{2+}$ featuring the same molecular bridge (Table 3). This difference points to significantly more Fe-centered oxidation of the Fe–C \equiv C termini, as also confirmed by DFT calculations (see below). The electronic interaction between the Fe centers in $[1b]^+$ through the TPA core becomes strongly limited, resulting in dominant disproportionation of the monocation to **1b** and $[1b]^{2+}$. Therefore, $[1b]^+$ is hardly detectable by IR spectroscopy (Table 3 and Supporting Information, Figures S5 and S6), and only the characteristic NIR absorption (Supporting Information, Figure S6) reveals its presence. The negligible change in the $\nu(\text{C}\equiv\text{C})$ wavenumber accompanying the third anodic step producing $[1b]^{3+}$ resembles the formation of $[1a]^{3+}$ (Figure 3), both bearing the TPA-core oxidation characteristics.

The UV–vis–NIR spectra of complexes **1a**, **1b**, and **2a** and TMS-terminated bridges **1d** and **2d** in the different oxidation states were recorded by using the spectro-electrochemical monitoring or stepwise chemical oxidation, as shown in Figures 4 and 5 and Supporting Information, Figures S7–S12. The relevant data are collected in Table 4.

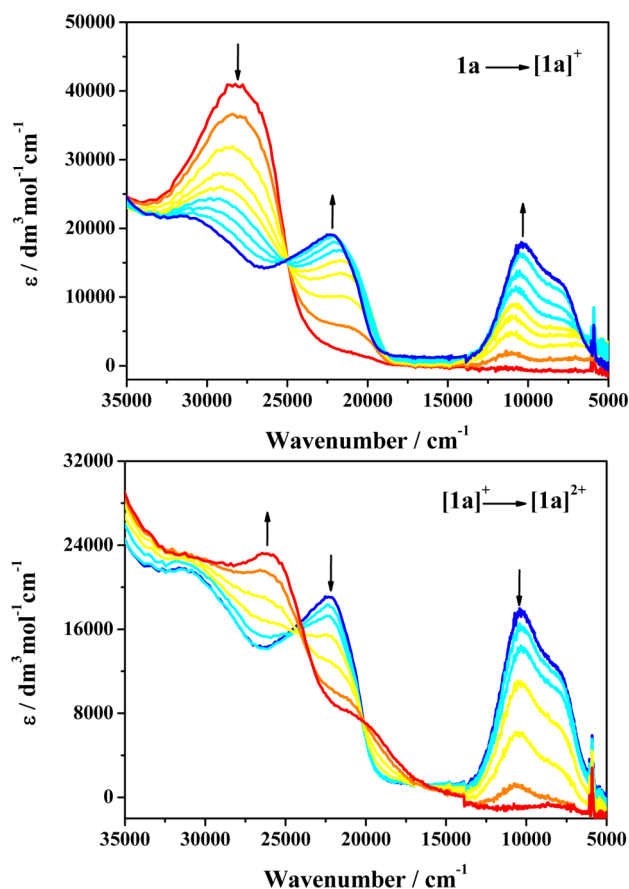


Figure 4. UV–vis–NIR spectral changes recorded during the oxidation of complex **1a** to $[1a]^+$ (top) and $[1a]^{2+}$ (bottom) in $\text{CH}_2\text{Cl}_2/1 \times 10^{-1}\text{ M } n\text{-Bu}_4\text{NPF}_6$ at 298 K within an OTTE cell.

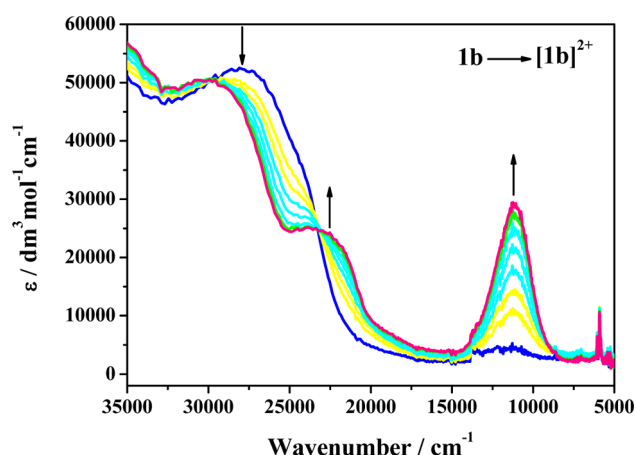


Figure 5. UV–vis–NIR spectral changes recorded during the oxidation of complex **1b** to $[1b]^{2+}$ in $\text{CH}_2\text{Cl}_2/1 \times 10^{-1}\text{ M } n\text{-Bu}_4\text{NPF}_6$ at 298 K within an OTTE cell.

Table 4. UV–Vis–NIR Electronic Absorption of Complexes **1a**, **1b**, **1d**, **2a**, **2d**, and Their Oxidized Forms in Dichloromethane/ $n\text{-Bu}_4\text{NPF}_6$

complex	$\tilde{\nu}_{\text{max}}$ (cm^{-1}) (ϵ_{max} ($\text{dm}^3\text{ mol}^{-1}\text{ cm}^{-1}$))
1a	28 100 (41 300)
$[1a]^+$	22 200 (19 500), 10 200 (18 100), 7800 (12 400)
$[1a]^{2+}$	26 000 (23 300), 20 500 (7600)
$[1a]^{3+}$	23 800 (21 900), 8300 (10 400)
1b	27 500 (52 700)
$[1b]^+$	^a
$[1b]^{2+}$	29 600 (50 800), 22 500 (24 700), 11 200 (29 400)
$[1b]^{3+}$	16 800 (32 000), 9700 (19 000)
1d	41 400 (28 600), 28 500 (40 700)
$[1d]^+$	13 500 (12 200)
2a	29 200 (56 600)
$[2a]^+$	^b 30 400, 21 600, 10 300, 8400sh
$[2a]^{2+}$	29 800 (44 700), 22 000 (8500)
$[2a]^{3+}$	23 900 (22 700), 8700 (22 200)
2d	29 600 (43 200)
$[2d]^+$	23 400 (23 600), 10 400 (19 100), 8100 (12 400)
$[2d]^{2+}$	38 600 (28 300), 13 900 (44 800)

^a Detectable by an unresolved weak NIR absorption between 10 000 and 4000 cm^{-1} (see Supporting Information, Figure S6). ^b Molar absorptivity not reported.

The diethynyl–TPA complex **1a** exhibits a pronounced broad absorption band at $\sim 2.8 \times 10^4\text{ cm}^{-1}$, most likely stemming from the $\pi \rightarrow \pi^*$ intraligand transition with some metal-to-ligand charge transfer contribution, in line with the reported similar systems.^{26–28} The smooth oxidation of neutral **1a** to $[1a]^+$ conformers leads to the appearance of new intense visible and NIR absorptions and strongly diminished parent UV absorption (Figure 4, top). The asymmetric NIR absorption of $[1a]^+$ corresponds to an overlap of two sub-bands obtained by deconvolution of the Gaussian function (Supporting Information, Figure S9 and Table S2). On further oxidation to dicationic species $[1a]^{2+}$, the characteristic NIR absorption of $[1a]^+$ gradually disappeared (Figure 4, bottom). The final, well-separated anodic step producing $[1a]^{3+}$ led to appearance of a new NIR absorption band below $1 \times 10^4\text{ cm}^{-1}$ (Figure S7) resembling the electronic absorption of oxidized reference $[1d]^+$ at $1.35 \times 10^4\text{ cm}^{-1}$ (Figure S10) and, therefore, belonging to the TPA radical cation.²⁹ It has to be considered

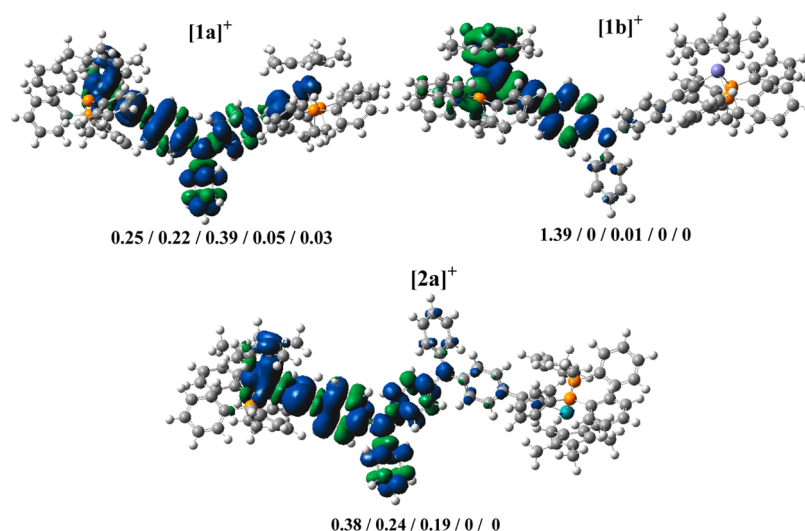


Figure 6. Calculated spin density distribution in $[1a]^+$ and $[2a]^+$ (Ru/C \equiv C/arylamine/C \equiv C/Ru), and $[1b]^+$ (Fe/C \equiv C/arylamine/C \equiv C/Fe). Contour values: ± 0.04 (e/bohr 3) $^{1/2}$. BLYP35/6-31G* (Ru/Fe: Lanl2DZ)/CPCM/CH $_2$ Cl $_2$.

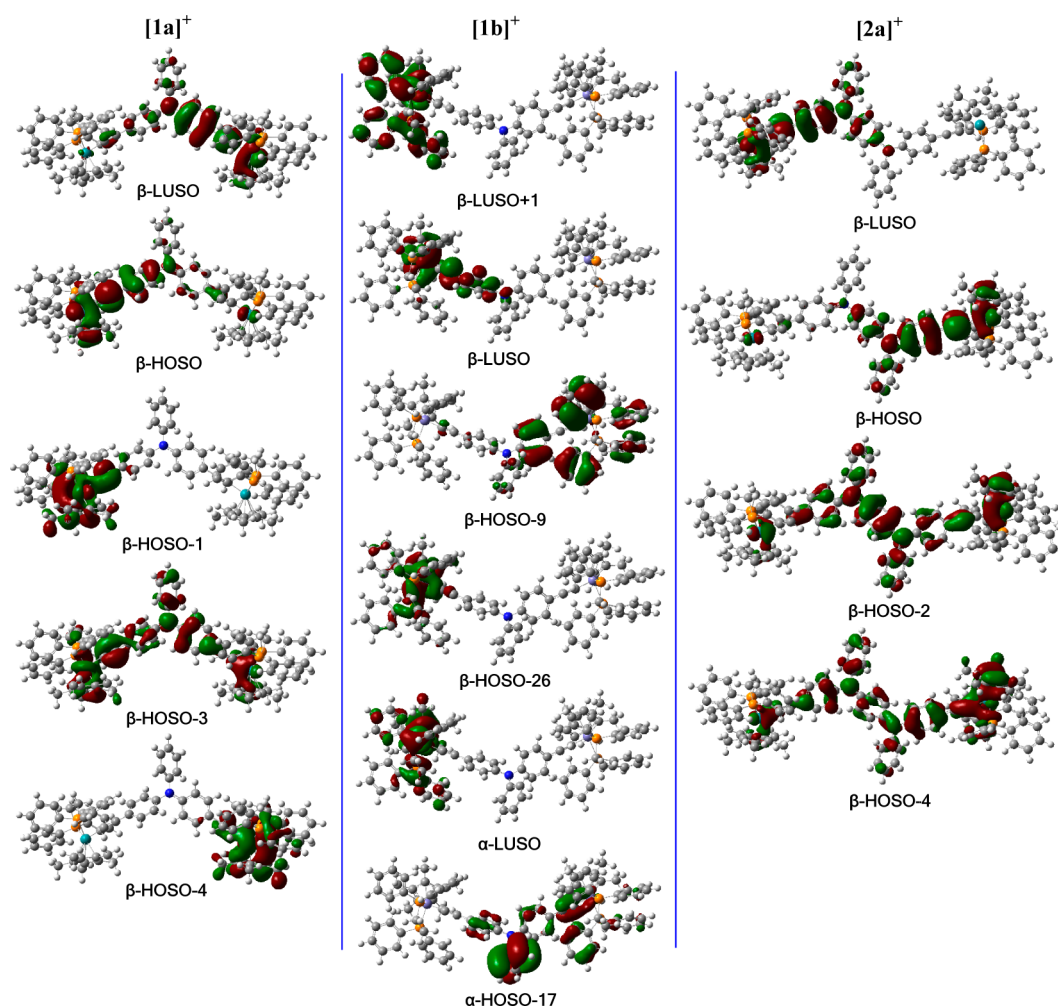


Figure 7. Spin orbitals involved in the major electronic excitations in $[1a]^+$ (left), $[1b]^+$ (middle), and $[2a]^+$ (right) presented in Table 5 (D = doublet). BLYP35/6-31G* (Ru/Fe: Lanl2DZ) /CPCM/CH $_2$ Cl $_2$.

that the oxidized Ru–C \equiv C units in precursor $[1a]^{2+}$ somewhat affects the absorption of the cationic bridge-core in $[1a]^{3+}$, causing its different position and band shape compared to $[1d]^+$. Thus, the third anodic step of **1a** is mainly localized

on the TPA core, in agreement with the foregoing voltammetric and IR spectro-electrochemical results.

The stepwise oxidation of **1b** to $[1b]^{2+}$ was accompanied by the instantaneous growth of an intense symmetric absorption

Table 5. Major Electronic Excitations in $[1a]^+$, $[1b]^+$, and $[2a]^+$ Determined by the TD-DFT Method^a

complex	excited state	λ (nm) [$\bar{\nu}$ (cm ⁻¹)]	osc strength (f)	major contributions	assignment	$\bar{\nu}$ (cm ⁻¹) (experiment)
$[1a]^+$	D_2	1306 [7655]	0.43	β -HOSO $\rightarrow\beta$ -LUSO (77%)	Ru(1)-C \equiv C(Ph) \rightarrow Ru(2)-C \equiv C(Ph) ⁺ IVCT/ ILET	7900
				β -HOSO-4 $\rightarrow\beta$ -LUSO (23%)	Ru(2) (dppe)Cp [*] \rightarrow Ru(2)-C \equiv C(Ph) ⁺ CT	
	D_4	807 [12 390]	0.10	β -HOSO-1 $\rightarrow\beta$ -LUSO (60%)	Cp [*] Ru(1)-C \equiv C \rightarrow Ru(2)-C \equiv C(Ph) ⁺ CT	10 400
				β -HOSO-3 $\rightarrow\beta$ -LUSO (33%)	Ru(1)-C \equiv C-TPA \rightarrow Ru(2)-C \equiv C(Ph) ⁺ CT	
$[1b]^+$	D_4	1051 [9515]	0.13	β -HOSO-26 $\rightarrow\beta$ -LUSO (49%)	Cp [*] (at Fe(2)) ⁺ \rightarrow Fe(2)-C \equiv C(Ph) ⁺ ILET	<10 000 (unresolved $\bar{\nu}_{\max}$)
				β -HOSO-9 $\rightarrow\beta$ -LUSO (38%)	Cp [*] (dppe)C \equiv C \rightarrow Fe(2)C \equiv C(Ph) ⁺ CT	
	D_{10}	568 [17 605]	0.029	β -HOSO-26 $\rightarrow\beta$ -LUSO+1 (32%)	Cp [*] (at Fe(2)) ⁺ \rightarrow dppe(at Fe(2)) ⁺	not observed
				α -HOSO-17 $\rightarrow\alpha$ -LUSO (32%)	TPA(C \equiv C) \rightarrow FeCp [*] (dppe) ⁺	
$[2a]^+$	D_3	1091 [9165]	0.14	β -HOSO-2 $\rightarrow\beta$ -LUSO (75%)	Ru(1)-C \equiv C-TPPD \rightarrow Ru(2)-C \equiv C(Ph) ⁺ ILET/IVCT	8400
				β -HOSO $\rightarrow\beta$ -LUSO (25%)	Ru(1)-C \equiv C(Ph) \rightarrow Ru(2)-C \equiv C(Ph) ⁺ IVCT/ ILET	
	D_6	661 [15 130]	0.061	β -HOSO-4 $\rightarrow\beta$ -LUSO (65%)	Ru(1)-C \equiv C-TPPD \rightarrow Ru(2)-C \equiv C(Ph) ⁺ ILET/IVCT	10 300
				β -HOSO-2 $\rightarrow\beta$ -LUSO (15%)	Ru(1)-C \equiv C-TPPD \rightarrow Ru(2)-C \equiv C(Ph) ⁺ ILET/IVCT	

^aThe DFT method was BLYP35/6-31G* (Ru/Fe: Lanl2DZ) /CPCM/CH₂Cl₂. D = doublet.

band at 1.12×10^4 cm⁻¹ (Figure 5), reflecting the redox disproportionation of $[1b]^+$ to the stable dication and parent **1b**, in agreement with the IR monitoring of the initial anodic process (see above). The low-energy absorption of $[1b]^{2+}$ is reminiscent of ligand-to-metal charge transfer transitions in formally Fe(III) complexes $[\{Fe(dppe)Cp^*(C\equiv C-)\}_n(Ph)]^{n+}$ ($n = 1, 2$).³⁰ The striking difference in the NIR electronic absorption between $[1b]^{2+}$ and $[1a]^{2+}$, combined with the poorly separated anodic waves in the former case, does not support participation of the TPA bridge core in the initial oxidation of **1b**. The latter process occurs probably during the subsequent well-separated oxidation of $[1b]^{2+}$ to $[1b]^{3+}$ (Figure S8), as indicated by the comparison with the similar electronic absorption of reference $[1d]^+$ (Figure S10) as well as the invariant IR $\nu(C\equiv C)$ band during this anodic step (Figure 3, right). The product of the initial one-electron oxidation step, $[1b]^+$, is hardly observable during the UV-vis-NIR spectroelectrochemical monitoring of the anodic conversion of **1b** to $[1b]^{2+}$ due to the aforementioned redox disproportionation process. However, the weak NIR absorption below 1.1×10^4 cm⁻¹, attributed to unstable $[1b]^+$, is clearly seen in the course of the chemical oxidation of **1b** with 1 equiv of FcPF₆ (Supporting Information, Figure S6); its assignment, different from an intervalence charge transfer (IVCT), is presented in the following theoretical (time-dependent (TD) DFT) section.

The observed characteristic UV-vis-NIR spectral changes resulting from the stepwise oxidation of TMS-terminated reference compound **2d** to the corresponding mono- and dication (Supporting Information, Figure S11) are fully consistent with the spectral evolution reported in the literature³¹ for bare TPPD lacking the ethynyl linkers. By contrast, the partly resolved first and second anodic steps of diruthenium diethynyl-TPPD complex **2a** gave rise to UV-vis-NIR absorption changes (Supporting Information, Figure S12) strongly resembling the generation of monocationic diethynyl-TPA-bridged species $[1a]^+$, which also matched

their similar IR $\nu(C\equiv C)$ shifts described in the preceding text. Stable $[2a]^{3+}$ is then characterized by a new UV-vis-NIR absorption (Figure S12, bottom) assigned to the oxidized radical-cationic TPPD core in $[2a]^{3+}$, which is evident from the comparison with the low-lying electronic absorption of reference $[2d]^+$ (Figure S11) as well as the negligible change in the $\nu(C\equiv C)$ wavenumber on oxidation of $[2a]^{2+}$ (Figure S3).

Theoretical Calculations. DFT calculations, using the BLYP35 functional, were performed to gain insight into the electronic structures of the one-electron-oxidized open-shell species $[1a]^+$, $[1b]^+$, and $[2a]^+$, although the latter two cations were not generated in the pure forms during the spectroelectrochemical experiments due to valence disproportionation equilibria resulting in their mixture with the corresponding dications. This applies especially for $[1b]^+$ detected only in a very small amount (Supporting Information, Figure S6). The basis set employed here is 6-31G* (Lanl2DZ for Ru and Fe atoms). The BLYP35 method reported by Kaupp and co-workers is appropriate for triarylamine and organometallic complexes similar to our systems.^{25,32} All the calculations were performed on nontruncated complexes $[1a]^+$, $[1b]^+$, and $[2a]^+$ to warrant their accuracy, regardless of the relatively heavy computing burden. To account also for solvent effects, the conductor polarizable continuum model (CPCM) in CH₂Cl₂ was employed for the ground-state structural optimization and analyses as well as in TD-DFT calculations of the electronic excitation energies. The pertinent data are presented in Figures 6 and 7, Supporting Information, Figures S13 and S14, and Table 5.

The DFT results indicate similar geometric changes taking place upon the one-electron oxidation of diruthenium complexes **1a** and **2a** (see Supporting Information, Figure S14). The anodic electron transfer results in dominant elongation of one of the C \equiv C bonds and shorter adjacent (ethynyl)C-Ru, (ethynyl)C-C(phenylene), and N-C-

(phenylene) bonds. The differences between the neutral and monocationic states are greater for **1a**. The diethynyl–TPA bridge is more involved in the initial oxidation of **1a** than the diethynyl–TPPD bridge in **2a**, in agreement with the larger separation of the first two anodic waves for **1a** (Figure 2 and Table 2) reflecting a stronger electronic interaction between the Ru centers mediated by the diethynyl–TPA bridge. In contrast, no significant changes in the bonding characteristics of the diethynyl–TPA bridge accompanied the model oxidation of **1b** that is localized exclusively on the metallic termini. The iron–Cp* centers oxidize independently, and the mixed-valence species, $[\mathbf{1b}]^+$, is unstable with respect to redox disproportionation and conversion to $[\mathbf{1b}]^{2+}$, as was revealed by the UV–vis–NIR spectroscopic monitoring of the anodic path. However, the experimental IR spectro-electrochemical results (Table 3) illustrate that the ethynyl linkers are still involved in the initial oxidation of **1b**, although much less than encountered in both diruthenium complexes, **1a** and **2a**.

The important complementary results obtained with DFT for the spin density distribution in $[\mathbf{1a}]^+$, $[\mathbf{1b}]^+$, and $[\mathbf{2a}]^+$ are shown in Figure 6. Apparently, the spin localization in $[\mathbf{1a}]^+$ and, increasingly, in $[\mathbf{2a}]^+$ and $[\mathbf{1b}]^+$ is asymmetric, residing largely on the ruthenium–ethynyl(–phenylene) and iron–Cp* redox centers, respectively, in one-half of the molecule, which is fully consistent with the symmetry-broken triple bond stretching induced by the initial oxidation of **1a**, **2a**, and **1b** (vide supra). Not surprisingly, the asymmetric spin of $[\mathbf{1a}]^+$ exhibits a delocalized distribution in contrast to the strongly localized oxidation of **1b**, again affirming the effect of the different metal centers on the anodic behavior.

Also worth mentioning is the difference in the spin distribution calculated for radical cations $[\mathbf{1a}]^+$ and $[\mathbf{2a}]^+$ featuring the different bridge cores (Figure 6). In contrast to the delocalized asymmetric spin distribution in $[\mathbf{1a}]^+$, the spin density in $[\mathbf{2a}]^+$ is localized more on one of the Ru centers and less on the bridge core, with no apparent involvement of the remote ruthenium–ethynyl unit, thereby matching well the weak electronic coupling between the ruthenium centers across the elongated TPPD bridge core in $[\mathbf{2a}]^+$ illustrated by the experimental results.

TD-DFT calculations were performed to reproduce the low-energy absorption features in the experimental UV–vis–NIR spectra of the monocationic diethynyl monoamine and diamine complexes and to facilitate their assignment in support of the spin-localized bonding situation (Figure 6). The relevant electronic transitions are presented in Table 5 and depicted in Figure 7. According to the TD-DFT results, the NIR band of $[\mathbf{1a}]^+$ at 7800 cm^{-1} (ν_2 in Figure S9 and Table S2, Supporting Information) has been well-duplicated and can mainly be attributed to the β -HOSO \rightarrow β -LUSO transition (HOSO = highest occupied system orbital; LUSO = lowest unoccupied system orbital). The β -HOSO is primarily localized on the nonoxidized Ru–C \equiv C unit (70%), imparting the corresponding transition an appreciable IVCT character. The electronic coupling parameter, $H_{ab} = 685\text{ cm}^{-1}$, was determined from the Hush formula, $H_{ab} = (2.06 \times 10^{-2}/R_{ab})(\epsilon_{\max}\nu_{\max}\Delta\nu)^{1/2}$ (ref 33), in which R_{ab} is the distance between the ruthenium centers in the X-ray crystal structure (Figure 1). Hence, $[\mathbf{1a}]^+$ can be classified as a moderately coupled Robin–Day Class II mixed-valence compound. The higher-lying electronic transition computed at $12\,390\text{ cm}^{-1}$ is most likely responsible for the absorption band of $[\mathbf{1a}]^+$ at $10\,200\text{ cm}^{-1}$ (ν_1 in Figure S9 and Table S2, Supporting Information). It involves both β -HOSO–I

and β -HOSO–3 so that the associated charge transfer to the oxidized Ru(2)–C \equiv C(Ph) $^+$ site of $[\mathbf{1a}]^+$ also involves the Cp*(Ru) and TPA donor sites.

Complex $[\mathbf{1b}]^+$ exhibits an NIR excitation at 9515 cm^{-1} belonging to β -HOSO–26 \rightarrow β -LUSO and β -HOSO–9 \rightarrow β -LUSO transitions. The dominant former component is localized at the oxidized metallic site, having a partial inter-configurational (IC) character typically observed for similar predominantly Fe(III) systems.^{24,34} The acceptor ethynyl(–phenylene) and donor Cp* frameworks are also involved. The second component represents a charge transfer from a ligand-based π -orbital delocalized in the nonoxidized half of $[\mathbf{1b}]^+$. A convincing experimental evidence for this low-energy electronic absorption in valence-localized $[\mathbf{1b}]^+$ with weakly interacting Fe centers is shown in Figure S6 (Supporting Information). The calculated visible electronic absorption of $[\mathbf{1b}]^+$ could not be verified experimentally (Figure 5 and Supporting Information, Figure S6) due to the redox disproportionation of the cation and the tailing absorption of $[\mathbf{1b}]^{2+}$ in that region.

The asymmetric NIR absorptions of $[\mathbf{2a}]^+$ at ca. 8400 and $10\,300\text{ cm}^{-1}$ have been reproduced less accurately than in the case of $[\mathbf{1a}]^+$, probably due to the exaggerated planar conformation of TPPD seen in the computed model. The calculated excitations encompass the dominant β -HOSO–2 \rightarrow β -LUSO and β -HOSO–4 \rightarrow β -LUSO transitions, respectively. Both β -HOSO–2 and β -HOSO–4 are delocalized over the planar TPPD core and the nonoxidized Ru–C \equiv C unit. Similar to $[\mathbf{1a}]^+$, the β -LUSO resides on the oxidized Ru(2)–C \equiv C(Ph) $^+$ site. The IVCT character of the lowest NIR absorption of $[\mathbf{2a}]^+$ becomes enhanced by the 25% admixture of the β -HOSO \rightarrow β -LUSO component.

CONCLUSIONS

The electrochemical results reveal that homo-bimetallic complexes **1a**, **1b**, and **2a** undergo multistep oxidation processes. The monocationic state of **1a** is stable, with a large K_c value compared to $[\mathbf{1b}]^+$ that tends to disproportionate to the corresponding dication. Likewise, instability was also expected for $[\mathbf{2a}]^+$ with the extended diamine bridge core, based on the similar poorly resolved first two anodic responses of **1b** and **2a**. However, $[\mathbf{2a}]^+$ could still readily be detected with in situ UV–vis–NIR spectroscopy, bearing a strong resemblance to $[\mathbf{1a}]^+$. Combined results of IR and UV/vis/NIR spectro-electrochemistry and DFT/TD-DFT calculations of nontruncated models have demonstrated that (i) there exists an appreciable electronic interaction between the two ruthenium centers in $[\mathbf{1a}]^+$; (ii) the first two oxidation steps of **1b** are largely Fe-localized; (iii) the spectroscopic characteristics of $[\mathbf{2a}]^+$ indicate much weaker electronic interaction between two ruthenium centers through the extended TPPD bridge core; (iv) the subsequent oxidation of the dications of **1a**, **1b**, and **2a** is localized on the arylamine bridge core (as revealed by IR spectro-electrochemistry and the comparison with the anodic behavior of the corresponding TMS-terminated derivatives). The elongated TPPD linker, with more twisted conformation and restricted π -conjugation, indeed, exhibits electronic insulation properties to some extent. Notably, a planar conformation of TPPD in $[\mathbf{2a}]^+$ and its stronger involvement in the initial oxidation than inferred from the experimental data have emerged from DFT calculations of the model complex. The alternative linear π -conjugated oligoarylamine structures will be the subject of our following report on long-range electron transfer systems. Furthermore, this work may

expedient for designing and investigating more diversified systems with multiple redox states.

EXPERIMENTAL SECTION

General Materials. All manipulations were performed under a dry argon gas atmosphere by using standard Schlenk techniques, unless stated otherwise. Solvents were predried and distilled under argon prior to use, except those used directly for spectroscopic measurements, which were of spectroscopic grade. The starting materials 4-bromo-*N*-(4-bromophenyl)-*N*-phenylaniline (**1c**),³⁵ *N*¹,*N*⁴-bis(4-bromophenyl)-*N*¹,*N*⁴-diphenylbenzene-1,4-diamine (**2c**),³⁶ [RuCl(dppe)Cp*],³⁷ and [FeCl(dppe)Cp*]³⁸ were prepared by the procedures described in the literature. Target complexes **1a–1b** and **2a** were prepared along the synthetic route presented in Scheme 1. Other reagents were purchased and used as received.

Syntheses. Intermediate 1d. To a stirred solution of precursor **1c** (806 mg, 2 mmol), CuI (38 mg, 0.2 mmol), and [Pd(PPh₃)₄] (231 mg, 0.2 mmol) in triethylamine (20 mL) and tetrahydrofuran (THF; 30 mL) under an argon atmosphere trimethylsilylacetylene (588 mg, 6 mmol) was added, and the mixture was held at 60 °C for 24 h. After it cooled, the solution was filtered through a bed of diatomaceous earth. The filtrate was evaporated under reduced pressure and purified by silica gel column chromatography (petroleum ether) to give a light yellow solid (753 mg, yield 86%). ¹H NMR (400 MHz, CDCl₃): δ 0.25 (s, 18H, SiMe₃), 6.96 (d, *J*_{HH} = 8 Hz, 4H, Ar–H), 7.06–7.11 (m, 4H, Ar–H), 7.32–7.34 (d, *J*_{HH} = 8 Hz, 5H, Ar–H). ¹³C NMR (100 MHz, CDCl₃): δ 0.03 (SiMe₃), 93.5, 105.1 (C≡C), 116.9, 123.1, 124.1, 124.9, 125.3, 129.3, 129.5, 133.0, 146.5, 147.3 (Ar), as reported in ref 39.

Intermediate 2d. Compound **2d** was prepared from precursor **2c** by a method analogous to that employed for **1d** and purified on a silica gel column (petroleum ether/dichloromethane = 10:1, v/v) to obtain a light yellow solid (980 mg, yield 81%). ¹H NMR (400 MHz, CDCl₃): δ 0.24 (s, 18H, SiMe₃), 6.98–7.10 (m, 14H, Ar–H), 7.28–7.31 (m, 8H, Ar–H). ¹³C NMR (100 MHz, CDCl₃): δ 0.28 (SiMe₃), 93.0, 105.3 (C≡C), 115.8, 121.8, 123.4, 124.7, 125.6, 129.3, 132.8, 142.4, 146.8, 147.7 (Ar). EI-MS: *m/z* = 604.55 [M]⁺. Anal. Calcd for C₄₀H₄₀N₂Si₂: C, 79.42; H, 6.66; N, 4.63. Found: C, 79.63; H, 6.58; N, 4.67%.

Homo-Bimetallic Complexes 1a, 1b, and 2a. Target compounds **1a**, **1b**, and **2a** were prepared along the synthetic route presented in Scheme 1.

[[Ru(dppe)Cp*(C≡C)]₂(μ-TPA)] (1a). A solution of [RuCl(dppe)Cp*] (321 mg, 0.50 mmol), **1d** (100 mg, 0.23 mmol), and KF (160 mg, 2.76 mmol) in CH₃OH (20 mL) and THF (5 mL) was heated to reflux under nitrogen atmosphere for 24 h. The crude product was collected by filtration and washed with hexane. The solid was dissolved in dichloromethane and precipitated by slow diffusion of hexane. The solid was filtered off and dried to give **1a** as a yellow powder (312 mg, yield 87%). ¹H NMR (400 MHz, CDCl₃): δ 1.56 (s, 30H, CH₃ of C₅Me₅), 2.03–2.08 (m, 4H, CH₂ of dppe), 2.66–2.71 (m, 4H, CH₂ of dppe), 6.65–6.76 (m, 8H, Ar–H), 6.86–6.87 (m, 1H, Ar–H), 6.99 (d, 2H, *J* = 8 Hz Ar–H), 7.13–7.35 (m, 34H, Ar–H), 7.79 (br, 8H, Ar–H). ¹³C NMR (100 MHz, CDCl₃): δ 10.1 (CH₃ of C₅Me₅), 29.2–31.6 (m, CH₂ of dppe), 92.4 (CH₃ of C₅Me₅), 109.1 (Ru–C≡C), 122.4 (Ru–C≡C), 123.9–148.3 (m, Ar). ³¹P NMR (160 MHz, CDCl₃): δ 78.97 (s, dppe). IR (KBr/cm^{−1}): ν (C≡C) 2062 (w). Anal. Calcd for C₉₄H₉₁NP₄Ru₂: C, 72.34; H, 5.88; N, 0.90. Found: C, 72.56; H, 5.78; N, 0.91%.

[[Fe(dppe)Cp*(C≡C)]₂(μ-TPA)] (1b). A solution of **1d** (87 mg, 0.20 mmol) and K₂CO₃ (61 mg, 0.44 mmol) in CH₃OH (30 mL) and THF (10 mL) was stirred for 10 h under nitrogen atmosphere at room temperature. Then, [FeCl(dppe)Cp*] (275 mg, 0.44 mmol) and Na[BPh₄] (151 mg, 0.44 mmol) were added. After 16 h of stirring, *t*BuOK (52 mg, 0.44 mmol) was introduced, and the mixture was stirred for another 4 h, after which the solvent was evaporated and the residue was extracted with toluene (4 × 10 mL). After the solvent removal, washing with pentane (3 × 10 mL), and vacuum drying, an orange powder was obtained (182 mg, 0.12 mmol, yield 62%). ¹H

NMR (400 MHz, CDCl₃): δ 1.41 (s, 30H, CH₃ of C₅Me₅), 1.96 (br, 4H, CH₂ of dppe), 2.64 (br, 4H, CH₂ of dppe), 6.69 (br, 4H, Ar–H), 6.81–6.83 (m, 5H, Ar–H), 7.02 (d, *J* = 8 Hz, 2H, Ar–H), 7.24–7.34 (m, 34H, Ar–H), 7.91 (br, 8H, Ar–H). ¹³C NMR (100 MHz, CDCl₃): δ 10.1 (CH₃ of C₅Me₅), 30.1–31.6 (m, CH₂ of dppe), 87.5 (CH₃ of C₅Me₅), 121.0 (Fe–C≡C), 122.9–138.7 (m, Ar), 142.9 (Fe–C≡C). ³¹P NMR (160 MHz, CDCl₃): δ 95.63 (s, dppe). IR (KBr/cm^{−1}): ν (C≡C) 2051 (w). Anal. Calcd for C₉₄H₉₁NP₄Fe₂: C, 76.79; H, 6.24; N, 0.95. Found: C, 76.82; H, 6.22; N, 0.96%.

[[Ru(dppe)Cp*(C≡C)]₂(μ-TPPD)] (2a). Complex **2a** was prepared by an analogous method as **1a**, using the following amounts: [RuCl(dppe)Cp*] (464 mg, 0.69 mmol), **2d** (200 mg, 0.33 mmol), and KF (273 mg, 3.96 mmol) dissolved in CH₃OH (20 mL), THF (5 mL). The product was obtained as a light green solid (353 mg, 62% yield). ¹H NMR (400 MHz, CDCl₃): δ 1.56 (s, 30H, CH₃ of C₅Me₅), 1.99–2.10 (m, 4H, CH₂ of dppe), 2.65–2.76 (m, 4H, CH₂ of dppe), 6.70 (d, 4H, *J* = 8 Hz, Ar–H), 6.79 (d, 4H, *J* = 8 Hz, Ar–H), 6.87–6.92 (m, 6H, Ar–H), 7.03 (d, 4H, *J* = 8 Hz Ar–H), 7.17–7.34 (m, 36H, Ar–H), 7.79 (br, 8H, Ar–H). ¹³C NMR (100 MHz, CDCl₃): δ 10.0 (CH₃ of C₅Me₅), 29.4–29.7 (m, CH₂ of dppe), 92.5 (CH₃ of C₅Me₅), 122.6 (Ru–C≡C), 122.9 (Ru–C≡C), 127.1–133.8 (m, Ar). ³¹P NMR (160 MHz, CDCl₃): δ 70.86 (s, dppe). IR (KBr/cm^{−1}): ν (C≡C) 2067 (s). Anal. Calcd for C₁₀₆H₁₀₀N₃P₄Ru₂: C, 73.68; H, 5.83; N, 1.62. Found: C, 73.59; H, 5.80; N, 1.61%.

X-ray Crystallography. Single crystals of complexes **1a** and **2a** suitable for X-ray analysis were grown by layering a solution in dichloromethane with hexane. Crystals with approximate dimensions of 0.20 × 0.20 × 0.10 mm³ for **1a** and 0.20 × 0.20 × 0.20 mm³ for **2a** were mounted on glass fibers for diffraction experiments. Intensity data were collected on a Nonius Kappa CCD diffractometer with Mo Kα radiation (0.710 73 Å) at room temperature. The crystal structures were determined by a combination of direct methods (SHELXS-97)⁴⁰ and Fourier difference techniques, and refined by full matrix least-squares (SHELXL-97).⁴¹ All non-H atoms were refined anisotropically. The hydrogen atoms were placed in ideal positions and refined as riding atoms. The partial solvent molecules were omitted. Further crystal data and details of the data collection are summarized in Table S1. Selected bond distances and angles are given in Table 1.

Physical Measurements. ¹H, ¹³C, and ³¹P NMR spectra were collected on a Varian Mercury Plus 400 spectrometer (400 MHz). ¹H and ¹³C NMR chemical shifts are relative to Si(CH₃)₄, and ³¹P NMR chemical shifts are relative to 85% H₃PO₄. Elemental analyses (C, H, N) were performed with a Vario EIII Chnso instrument. The electrochemical measurements were performed on a CHI 660C potentiostat. A three-electrode single-compartment cell was used for the solution of complexes and supporting electrolyte in dry CH₂Cl₂. The solution was deaerated by argon bubbling on a frit for ~10 min before the measurement. The analyte (complex, ligand) and electrolyte (*n*-Bu₄NPF₆) concentrations were typically 1 × 10^{−3} and 1 × 10^{−1} mol dm^{−3}, respectively. A prepolished 500 μm diameter platinum disk working electrode, a platinum wire counter electrode, and an Ag wire pseudoreference electrode were used. Ferrocene was used as the internal potential reference. Spectro-electrochemical experiments at room temperature were performed with an airtight optically transparent thin-layer electrochemical (OTTLE) cell (optical path length of ca. 200 μm) equipped with a Pt minigrid working electrode and CaF₂ windows.⁴² The cell was positioned in the sample compartment of a Bruker Tensor Fourier transform IR spectrometer (1 cm^{−1} spectral resolution, eight scans) or a Shimadzu UV-3600 UV–vis–NIR spectro-photometer. The controlled-potential electrolyses were performed with a CHI 660C potentiostat. The concentration of analyte samples was ca. 2 × 10^{−3} mol dm^{−3}. Dry 3 × 10^{−1} M *n*-Bu₄NPF₆ was used as the supporting electrolyte.

Computational Details. DFT calculations were performed with the Gaussian 09 program,⁴³ at the BLYP35/6-31G* level of theory. The basis set employed was 6-31G* (Lanl2DZ for Ru and Fe atoms). Geometry optimization was performed without any symmetry constraints. Electronic transitions were calculated by the TD-DFT method. The molecular orbital contributions were generated using the Multiwfn package and plotted using GaussView 5.0. The solution

651 effects in dichloromethane are included for a part of the calculations
652 with the CPCM.⁴⁵

653 ■ ASSOCIATED CONTENT

654 ⓘ Supporting Information

655 The Supporting Information is available free of charge on the
656 ACS Publications website at DOI: 10.1021/acs.inorg-
657 chem.6b02809.

658 Crystallographic information, additional spectro-electro-
659 chemical information, additional calculated DFT data,
660 ¹H, ¹³C and ³¹P NMR spectra of the new compounds.
661 (PDF)

662 Crystallographic data (CIF)

663 Crystallographic data (CIF)

664 ■ AUTHOR INFORMATION

665 Corresponding Authors

666 *E-mail: f.hartl@reading.ac.uk. (F.H.)

667 *E-mail: chshliu@mail.ccnu.edu.cn. (S.H.L.)

668 ORCID

669 František Hartl: 0000-0002-7013-5360

670 Notes

671 The authors declare no competing financial interest.

672 ORCID, Frantisek Hartl: 0000-0002-7013-5360

673 ■ ACKNOWLEDGMENTS

674 The authors acknowledge financial support from National
675 Natural Science Foundation of China (21272088, 21472059,
676 21402057), the self-determined research funds of the CCNU
677 from the colleges' basic research and operation of MOE
678 (CCNU14A05009, CCNU14F01003), and the Excellent
679 Doctoral Dissertation Cultivation Grant from the Central
680 China Normal University (2015YBYB108, 2016YBZZ040).

681 ■ REFERENCES

- 682 (1) (a) Ren, T. Diruthenium σ -alkynyl compounds: a new class of
683 conjugated organometallics. *Organometallics* **2005**, *24*, 4854–4870.
684 (b) Qi, H.; Noll, B.; Snider, G. L.; Lu, Y.; Lent, S. S.; Fehlnert, T. P.;
685 Gupta, A. Dependence of field switched ordered arrays of dinuclear
686 mixed-valence complexes on the distance between the redox centers
687 and the size of the counterions. *J. Am. Chem. Soc.* **2005**, *127*, 15218–
688 15227. (c) Schwab, P. F. H.; Smith, J. R.; Michl, J. Synthesis and
689 properties of molecular rods. 2. Zig-zag rods. *Chem. Rev.* **2005**, *105*,
690 1197–1279. (d) Burgun, A.; Ellis, B. G.; Roisnel, T.; Skelton, B. W.;
691 Bruce, M. I.; Lapinte, C. From molecular wires to molecular resistors:
692 TCNE, a class-III/class-II mixed-valence chemical switch. *Organo-*
693 *metallics* **2014**, *33*, 4209–4219. (e) Blum, A. S.; Ren, T.; Parish, D. A.;
694 Trammell, S. A.; Moore, M. H.; Kushmerick, J. G.; Xu, G. L.;
695 Deschamps, J. R.; Pollack, S. K.; Shashidhar, R. Ru₂(ap)₄ (σ -
696 oligo(phenyleneethynyl)) molecular wires: synthesis and electronic
697 characterization. *J. Am. Chem. Soc.* **2005**, *127*, 10010–10011.
698 (2) (a) Crutchley, R. J. Intervalence charge transfer and electron
699 exchange studies of dinuclear ruthenium complexes. *Adv. Inorg. Chem.*
700 **1994**, *41*, 273–325. (b) Schwab, P. F. H.; Levin, M. D.; Michl, J.
701 Molecular rods. 1. Simple axial rods. *Chem. Rev.* **1999**, *99*, 1863–1933.
702 (c) Xu, G. L.; Crutchley, R. J.; DeRosa, M. C.; Pan, Q. J.; Zhang, H. X.;
703 Wang, X.; Ren, T. Strong electronic couplings between ferrocenyl
704 centers mediated by bis-ethynyl/butadiynyl diruthenium bridges. *J.*
705 *Am. Chem. Soc.* **2005**, *127*, 13354–13365. (d) Zhu, X. X.; Ou, Y. P.;
706 Zhang, J.; Xia, J. L.; Yin, J.; Yu, G.-A.; Liu, S. H. Dithia[3.3]-
707 paracyclophane-based monometal ruthenium acetylide complexes:
708 synthesis, characterization and substituent effects. *Dalton Trans.*
709 **2013**, *42*, 7177–7189. (e) Xia, J. L.; Man, W. Y.; Zhu, X.; Zhang,
710 C.; Jin, G.; Schauer, P. A.; Fox, M. A.; Yin, J.; Yu, G.; Low, P. J.; Liu, S.

- H. Synthesis and characterization of dithia[3.3]paracyclophane-
711 bridged binuclear ruthenium vinyl and alkynyl complexes. *Organo-*
712 *metallics* **2012**, *31*, 5321–5333. (f) Man, W. Y.; Xia, J. L.; Brown, N. J.;
713 Farmer, J. D.; Yufit, D. S.; Howard, J. A. K.; Liu, S. H.; Low, P. J.
714 Spectroscopic and computational studies of the ligand redox non-
715 innocence in mono- and binuclear ruthenium vinyl complexes. *716*
Organometallics **2011**, *30*, 1852–1858. (g) Ou, Y. P.; Zhang, J.; Xu,
717 M.; Xia, J. L.; Hartl, F.; Yin, J.; Yu, G. A.; Liu, S. H. Bridge-localized
718 HOMO-binding character of divinyanthracene-bridged dinuclear
719 ruthenium carbonyl complexes: spectroscopic, spectroelectrochemical,
720 and computational studies. *Chem. - Asian J.* **2014**, *9*, 1152–1160.
721 (h) Ou, Y. P.; Zhang, J.; Zhang, F.; Kuang, D.; Hartl, F.; Rao, L.; Liu,
722 S. H. Notable differences between oxidized diruthenium complexes
723 bridged by four isomeric diethynyl benzodithiophene ligands. *Dalton*
724 *Trans.* **2016**, *45*, 6503–6516. (i) Ou, Y. P.; Xia, J. L.; Zhang, J.; Xu, M.;
725 Yin, J.; Yu, G. A.; Liu, S. H. Experimental and theoretical studies of
726 charge delocalization in biruthenium-alkynyl complexes bridged by
727 thiophenes. *Chem. - Asian J.* **2013**, *8*, 2023–2032. 728
(3) (a) Kaim, W. Concepts for metal complex chromophores
729 absorbing in the near infrared. *Coord. Chem. Rev.* **2011**, *255*, 2503–
730 2513. (b) Costuas, K.; Rigaut, S. Polynuclear carbon-rich organo-
731 metallic complexes: clarification of the role of the bridging ligand in
732 the redox properties. *Dalton Trans.* **2011**, *40*, S643–S658. (c) Halet, J.-
733 F.; Lapinte, C. Charge delocalization vs localization in carbon-rich iron
734 mixed-valence complexes: A subtle interplay between the carbon
735 spacer and the (dppe)Cp*Fe organometallic electrophore. *Coord.*
736 *Chem. Rev.* **2013**, *257*, 1584–1613. (d) Cao, Z.; Xi, B.; Jodoin, D. S.;
737 Zhang, L.; Cummings, S. P.; Gao, Y.; Tyler, S. F.; Fanwick, P. E.;
738 Crutchley, R. J.; Ren, T. Diruthenium-polyyn-diyl-diruthenium
739 wires: electronic coupling in the long distance regime. *J. Am. Chem.*
740 *Soc.* **2014**, *136*, 12174–12183. (e) Brunschwig, B. S.; Creutz, C.; Sutin,
741 N. Electroabsorption spectroscopy of charge transfer states of
742 transition metal complexes. *Coord. Chem. Rev.* **1998**, *177*, 61–79.
743 (f) Scheerer, S.; Rothowe, N.; Abdel-Rahman, O. S.; He, X.; Rigaut,
744 S.; Kvapilová, H.; Winter, R. F.; et al. Vinyl ruthenium-modified
745 biphenyl and 2, 2'-bipyridines. *Inorg. Chem.* **2015**, *54*, 3387–3402.
746 (g) Launay, J.-P. Long-distance intervalence electron transfer. *Chem.*
747 *Soc. Rev.* **2001**, *30*, 386–397. 748
(4) (a) Carroll, R. L.; Gorman, C. B. The genesis of molecular
749 electronics. *Angew. Chem., Int. Ed.* **2002**, *41*, 4378–4400. (b) Bennis-
750 ton, A. C. Pushing around electrons: towards 2-D and 3-D molecular
751 switches. *Chem. Soc. Rev.* **2004**, *33*, 573–578. (c) Gluyas, J. B. G.;
752 Boden, A. J.; Eaves, S. G.; Yu, H.; Low, P. J. Cross-conjugated systems
753 based on an (E)-hexa-3-en-1,5-diyne-3,4-diyl skeleton: spectroscopic
754 and spectroelectrochemical investigations. *Dalton Trans.* **2014**, *43*,
755 6291–6294. (d) Paul, F.; Lapinte, C. Organometallic molecular wires
756 and other nanoscale-sized devices: an approach using the organoiron
757 (dppe)Cp*Fe building block. *Coord. Chem. Rev.* **1998**, *178–180*, 431–
758 509. (e) Martin, R. E.; Diederich, F. Lineare monodisperse π -
759 konjugierte oligomere: mehr als nur modellverbindungen für
760 polymere. *Angew. Chem.* **1999**, *111*, 1440–1469. (f) Martin, R. E.;
761 Diederich, F. Linear monodisperse π -conjugated oligomers: model
762 compounds for polymers and more. *Angew. Chem., Int. Ed.* **1999**, *38*,
763 1350–1377. (g) Yao, C.-J.; Zhong, Y.-W.; Yao, J. N. Charge
764 delocalization in a cyclometalated bisruthenium complex bridged by
765 a noninnocent 1,2,4,5-tetra(2-pyridyl)benzene ligand. *J. Am. Chem.*
766 *Soc.* **2011**, *133*, 15697–15706. (h) Maurer, J.; Sarkar, B.; Schwederski,
767 B.; Kaim, W.; Winter, R. F.; Zálaiš, S. Divinylphenylene-bridged
768 diruthenium complexes bearing Ru(CO)Cl(P^tPr₃)₂ entities. *Organo-*
769 *metallics* **2006**, *25*, 3701–3712. (i) Pevny, F.; Di Piazza, E.; Norel, L.;
770 Drescher, M.; Winter, R. F.; Rigaut, S. Fully delocalized (ethynyl)
771 (vinyl) phenylene-bridged diruthenium radical complexes. *Organo-*
772 *metallics* **2010**, *29*, 5912–5918. 773
(5) (a) Whittall, I. R.; McDonagh, A. M.; Humphrey, M. G.; Marek,
774 S. Organometallic complexes in nonlinear optics II: third-order
775 nonlinearities and optical limiting studies. *Adv. Organomet. Chem.* **776**
1999, *43*, 349–405. (b) Mayor, M.; von Hänisch, C.; Weber, H. B.;
777 Reichert, J.; Beckmann, D. Ein trans-Platin (II)-Komplex als
778 Einzelmolekülisolator. *Angew. Chem.* **2002**, *114*, 1228–1231. 779

- (c) Mayor, M.; von Hänisch, C.; Weber, H. B.; Reichert, J.; Beckmann, D. A trans-platinum (II) complex as a single-molecule insulator. *Angew. Chem., Int. Ed.* **2002**, *41*, 1183–1186. (d) Schull, T. L.; Kushmerick, J. G.; Patterson, C. H.; George, C.; Moore, M. H.; Pollack, S. K.; Shashidhar, R. Ligand effects on charge transport in platinum (II) acetylides. *J. Am. Chem. Soc.* **2003**, *125*, 3202–3203. (e) Pfaff, U.; Hildebrandt, A.; Korb, M.; Lang, H. The influence of an ethynyl spacer on the electronic properties in 2, 5-ferrocenyl-substituted heterocycles. *Polyhedron* **2015**, *86*, 2–9. (f) Miesel, D.; Hildebrandt, A.; Korb, M.; Wild, D. A.; Low, P. J.; Lang, H. Influence of P-bonded bulky substituents on electronic interactions in ferrocenyl-substituted phospholes. *Chem. - Eur. J.* **2015**, *21*, 11545–11559. (g) Gidron, O.; Diskin-Posner, Y.; Bendikov, M. High charge delocalization and conjugation in oligofuran molecular wires. *Chem. - Eur. J.* **2013**, *19*, 13140–13150.
- (6) (a) Maurer, J.; Linseis, M.; Sarkar, B.; Schwederski, B.; Niemeyer, M.; Kaim, W.; Zálaiš, S.; Anson, C.; Zabel, M.; Winter, R. F. Ruthenium complexes with vinyl, styryl, and vinylpyrenyl ligands: A case of non-innocence in organometallic chemistry. *J. Am. Chem. Soc.* **2008**, *130*, 259–268. (b) Linseis, M.; Zálaiš, S.; Zabel, M.; Winter, R. F. Ruthenium stilbenyl and diruthenium distyrylene complexes: aspects of electron delocalization and electrocatalyzed isomerization of the Z-isomer. *J. Am. Chem. Soc.* **2012**, *134*, 16671–16692. (c) Zálaiš, S.; Winter, R. F.; Kaim, W. Quantum chemical interpretation of redox properties of ruthenium complexes with vinyl and TCNX type non-innocent ligands. *Coord. Chem. Rev.* **2010**, *254*, 1383–1396. (d) Lloveras, V.; Caballero, A.; Tárraga, A.; Velasco, M. D.; Espinosa, A.; Wurst, K.; Evans, D. J.; Vidal-Gancedo, J.; Rovira, C.; Molina, P.; Veciana, J. Synthesis and characterization of radical cations derived from mono- and bisferrocenyl-substituted 2-aza-1, 3-butadienes: a study of the influence of an asymmetric and oxidizable bridge on intramolecular electron transfer. *Eur. J. Inorg. Chem.* **2005**, *2005*, 2436–2450.
- (7) (a) Creutz, C.; Taube, H. Direct approach to measuring the Franck-Condon barrier to electron transfer between metal ions. *J. Am. Chem. Soc.* **1969**, *91*, 3988–3989. (b) Creutz, C.; Taube, H. Binuclear complexes of ruthenium ammines. *J. Am. Chem. Soc.* **1973**, *95*, 1086–1094. (c) Demadis, K. D.; Hartshorn, C. M.; Meyer, T. J. The localized-to-delocalized transition in mixed-valence chemistry. *Chem. Rev.* **2001**, *101*, 2655–2686. (d) Nelsen, S. F. "Almost Delocalized" Intervalence Compounds. *Chem. - Eur. J.* **2000**, *6*, 581–588. (e) Yamamoto, M.; Onitsuka, K.; Uno, M.; Takahashi, S. Synthesis of enantiopure planar-chiral cyclopentadienyl-ruthenium binuclear complexes bridged by aromatic systems. *J. Chem. Soc., Dalton Trans.* **2002**, 1473–1478. (f) Onitsuka, K.; Harada, Y.; Takahashi, S. Synthesis and properties of chiral organometallic polymers with (R)-3,3'-diethynyl-1,1'-binaphthyl bridges. *Synth. Met.* **2009**, *159*, 982–985.
- (8) (a) Tanaka, Y.; Shaw-Taberlet, J. A.; Justaud, F.; Cador, O.; Roisnel, T.; Akita, M.; Hamon, J.-R.; Lapinte, C. Electronic and magnetic couplings in free and π -coordinated 1,4-diethynyl-naphthalene-bridged $[\text{Cp}^*(\text{dppe})\text{Fe}]^{n+}$ ($n = 0, 1$) units. *Organometallics* **2009**, *28*, 4656–4669. (b) Low, P. J. Twists and turns: studies of the complexes and properties of bimetallic complexes featuring phenylene ethynylene and related bridging ligands. *Coord. Chem. Rev.* **2013**, *257*, 1507–1532. (c) Gao, L.-B.; Kan, J.; Fan, Y.; Zhang, L.-Y.; Liu, S.-H.; Chen, Z.-N. Wirelike dinuclear ruthenium complexes connected by bis(ethynyl)oligothiophene. *Inorg. Chem.* **2007**, *46*, 5651–5664. (d) Low, P. J. Metal complexes in molecular electronics: progress and possibilities. *Dalton Trans.* **2005**, 2821–2824. (e) Akita, M.; Koike, T. Chemistry of polycarbon species: from clusters to molecular devices. *Dalton Trans.* **2008**, 3523–3530. (f) Ying, J.-W.; Liu, I. P. C.; Xi, B.; Song, Y.; Campana, C.; Zuo, J.-L.; Ren, T. Linear trimer of diruthenium linked by butadiene-diyl units: a unique electronic wire. *Angew. Chem., Int. Ed.* **2010**, *49*, 954–957. (g) Fan, Y.; Zhang, L.-Y.; Dai, F.-R.; Shi, L.-X.; Chen, Z.-N. Preparation, characterization, and photophysical properties of Pt-M ($M = \text{Ru}, \text{Re}$) heteronuclear complexes with 1,10-phenanthrolineethynyl ligands. *Inorg. Chem.* **2008**, *47*, 2811–2819.
- (9) (a) Li, D.; Sun, X.; Wang, M.; Yu, H.; Zhou, H.; Wu, J.; Tian, Y. Novel colorimetric detection probe for copper (II) ions based on triphenylamine mixed-valence chromophores bearing prodigious two-photon absorption activity. *Sens. Actuators, B* **2015**, *220*, 1006–1016. (b) Rovira, C.; Ruiz-Molina, D.; Elsner, O.; Vidal-Gancedo, J.; Bonvoisin, J.; Launay, J. P.; Veciana, J. Influence of topology on the long-range electron-transfer phenomenon. *Chem. - Eur. J.* **2001**, *7*, 240–250. (c) Gautier, N.; Dumur, F.; Lloveras, V.; Vidal-Gancedo, J.; Veciana, J.; Rovira, C.; Hudhomme, P. Intramolecular electron transfer mediated by a tetrathiafulvalene bridge in a purely organic mixed-valence system. *Angew. Chem.* **2003**, *115*, 2871–2874. (d) Lindeman, S. V.; Rosokha, S. V.; Sun, D.; Kochi, J. K. X-ray structure analysis and the intervalent electron transfer in organic mixed-valence crystals with bridged aromatic cation radicals. *J. Am. Chem. Soc.* **2002**, *124*, 843–855. (e) Rosokha, S. V.; Sun, D. L.; Kochi, J. K. Conformation, distance, and connectivity effects on intramolecular electron transfer between phenylene-bridged aromatic redox centers. *J. Phys. Chem. A* **2002**, *106*, 2283–2292. (f) Bailey, S. E.; Zink, J. I.; Nelsen, S. F. Contributions of symmetric and asymmetric normal coordinates to the intervalence electronic absorption and resonance raman spectra of a strongly coupled p-phenylenediamine radical cation. *J. Am. Chem. Soc.* **2003**, *125*, 5939–5947.
- (10) (a) Nelsen, S. F.; Konradsson, A. E.; Weaver, M. N.; Telo, J. P. Intervalence near-IR spectra of delocalized dinitroaromatic radical anions. *J. Am. Chem. Soc.* **2003**, *125*, 12493–12501. (b) Mayor, M.; Büschel, M.; Fromm, K. M.; Lehn, J. M.; Daub, J. Electron transfer through molecular bridges between reducible pentakis(thiophenyl) benzene subunits. *Chem. - Eur. J.* **2001**, *7*, 1266–1272. (c) D'Alessandro, D. M.; Topley, A. C.; Davies, M. S.; Keene, F. R. Probing the transition between the localised (Class II) and localized-to-delocalised (Class II-III) regimes by using intervalence charge-transfer solvatochromism in a series of mixed-valence dinuclear ruthenium complexes. *Chem. - Eur. J.* **2006**, *12*, 4873–4884.
- (11) (a) Heckmann, A.; Amthor, S.; Lambert, C. Mulliken–Hush analysis of a bis (triarylamine) mixed-valence system with a N $\bullet\bullet\bullet$ N distance of 28.7 Å. *Chem. Commun.* **2006**, 2959–2961. (b) Hanss, D.; Walther, M. E.; Wenger, O. S. Importance of covalence, conformational effects and tunneling-barrier heights for long-range electron transfer: insights from dyads with oligo-p-phenylene, oligo-p-xylene and oligo-p-dimethoxybenzene bridges. *Coord. Chem. Rev.* **2010**, *254*, 2584–2592. (c) Banerjee, M.; Shukla, R.; Rathore, R. Synthesis, optical, and electronic properties of soluble poly-p-phenylene oligomers as models for molecular wires. *J. Am. Chem. Soc.* **2009**, *131*, 1780–1786. (d) Garmshausen, Y.; Schwarz, J.; Hildebrandt, J.; Kobin, B.; Pätz, M.; Hecht, S. Making nonsymmetrical bricks: synthesis of insoluble dipolar sexiphenyls. *Org. Lett.* **2014**, *16*, 2838–2841. (e) Miyata, Y.; Nishinaga, T.; Komatsu, K. Synthesis and structural, electronic, and optical properties of oligo(thienylfuran)s in comparison with oligothiophenes and oligofurans. *J. Org. Chem.* **2005**, *70*, 1147–1153.
- (12) (a) Polit, W.; Mücke, P.; Wuttke, E.; Exner, T.; Winter, R. F. Charge and spin confinement to the amine site in 3-connected triarylamine vinyl ruthenium conjugates. *Organometallics* **2013**, *32*, 5461–5472. (b) Dapperheld, S.; Steckhan, E.; Brinkhaus, K. H. G.; Esch, T. Organic electron transfer systems, II substituted triarylamine cation-radical redox systems-synthesis, electrochemical and spectroscopic properties, Hammett behavior, and suitability as redox catalysts. *Chem. Ber.* **1991**, *124*, 2557–2567. (c) Bender, T. P.; Graham, J. F.; Duff, J. M. Effect of substitution on the electrochemical and xerographic properties of triarylamines: correlation to the Hammett parameter of the substituent and calculated HOMO energy level. *Chem. Mater.* **2001**, *13*, 4105–4111. (d) Walter, R. I. Substituent effects on the properties of stable aromatic free radicals. The criterion for non-hammett behavior I. *J. Am. Chem. Soc.* **1966**, *88*, 1923–1930. (e) Amthor, S.; Noller, B.; Lambert, C. UV/Vis/NIR spectral properties of triarylamines and their corresponding radical cations. *Chem. Phys.* **2005**, *316*, 141–152.
- (13) (a) Connelly, N. G.; Geiger, W. E. Chemical redox agents for organometallic chemistry. *Chem. Rev.* **1996**, *96*, 877–910. (b) Tang, C. 917

- 918 W.; VanSlyke, A. S. Organic electroluminescent diodes. *Appl. Phys. Lett.* **1987**, *51*, 913–915. (c) Law, K. Y. Organic photoconductive materials: recent trends and developments. *Chem. Rev.* **1993**, *93*, 449–406.
- 922 (14) (a) Haridas, K. R.; Ostrauskaite, J.; Thelakkat, M.; Heim, M.; Bilke, R.; Haarer, D. Synthesis of low melting hole conductor systems based on triarylamines and application in dye sensitized solar cells. *Synth. Met.* **2001**, *121*, 1573–1574. (b) Bacher, E.; Bayerl, M.; Rudati, P.; Reckfuss, N.; Mueller, C. D.; Meerholz, K.; Nuyken, O. Synthesis and characterization of photo-cross-linkable hole-conducting polymers. *Macromolecules* **2005**, *38*, 1640–1647. (c) Kido, J.; Kimura, M.; Nagai, K. Multilayer white light-emitting organic electroluminescent device. *Science* **1995**, *267*, 1332–1334. (d) Gu, G.; Bulović, V.; Burrows, P. E.; Forrest, S. R.; Thompson, M. E. Transparent organic light emitting devices. *Appl. Phys. Lett.* **1996**, *68*, 2606–2608. (e) Cremer, J.; Bauerle, P.; Wienk, M. M.; Janssen, R. A. J. High open-circuit voltage poly(ethynylene bithienylene):fullerene solar cells. *Chem. Mater.* **2006**, *18*, 5832–5834. (f) Moerner, W. E.; Silence, S. M. Polymeric photorefractive materials. *Chem. Rev.* **1994**, *94*, 127–155. (g) Yen, H. J.; Guo, S. M.; Liou, G. S.; Chung, J. C.; Liu, Y. C.; Lu, Y. F.; Zeng, Y. Z. Mixed-valence class I transition and electrochemistry of bis-(triphenylamine)-based aramids containing isolated ether-linkage. *J. Polym. Sci., Part A: Polym. Chem.* **2011**, *49*, 3805–3816.
- 941 (15) (a) Zhou, G.; Baumgarten, M.; Mullen, K. Arylamine-substituted oligo(ladder-type pentaphenylene)s: electronic communication between bridged redox centers. *J. Am. Chem. Soc.* **2007**, *129*, 12211–12221. (b) Lambert, C.; Risko, C.; Coropceanu, V.; Schelter, J.; Amthor, S.; Gruhn, N. E.; Durivage, J. C.; Brédas, J.-L. Electronic coupling in tetraanisylarylenediamine mixed-valence systems: The interplay between bridge energy and geometric factors. *J. Am. Chem. Soc.* **2005**, *127*, 8508–8516. (c) Lancaster, K.; Odom, S. A.; Jones, S. C.; Thayumanavan, S.; Marder, S. R.; Brédas, J.-L.; Coropceanu, V.; Barlow, S. Intramolecular electron-transfer rates in mixed-valence triarylamines: measurement by variable-temperature ESR spectroscopy and comparison with optical data. *J. Am. Chem. Soc.* **2009**, *131*, 1717–1723. (d) Seo, E. T.; Nelson, R. F.; Fritsch, J. M.; Marcoux, L. S.; Leedy, D. W.; Adams, R. N. Anodic oxidation pathways of aromatic amines. Electrochemical and electron paramagnetic resonance studies. *J. Am. Chem. Soc.* **1966**, *88*, 3498–3503.
- 957 (16) (a) Hankache, J.; Wenger, O. S. Organic mixed valence. *Chem. Rev.* **2011**, *111*, 5138–5178. (b) Ramírez, C. L.; Pegoraro, C. N.; Filevich, O.; Bruttomesso, A.; Etchenique, R.; Parise, A. R. Role of ruthenium oxidation states in ligand-to-ligand charge transfer processes. *Inorg. Chem.* **2012**, *51*, 1261–1268. (c) Parthey, M.; Vincent, K. B.; Schauer, M. R. P. A.; Yufit, D. S.; Howard, J. A. K.; Kaupp, M.; Low, P. J.; Renz, M. A Combined computational and spectroelectrochemical study of platinum-bridged bis-triarylamine systems. *Inorg. Chem.* **2014**, *53*, 1544–1554. (d) Lambert, C.; Amthor, S.; Schelter, J. From valence trapped to valence delocalized by bridge state modification in bis(triarylamine) radical cations: evaluation of coupling matrix elements in a three-level system. *J. Phys. Chem. A* **2004**, *108*, 6474–6486. (e) Seibt, J.; Schaumlöffel, A.; Lambert, C.; Engel, V. Quantum study of the absorption spectroscopy of bis(triarylamine) radical cations. *J. Phys. Chem. A* **2008**, *112*, 10178–10184. (f) Heckmann, A.; Lambert, C. Organic mixed-valence compounds: a playground for electrons and holes. *Angew. Chem., Int. Ed.* **2012**, *51*, 326–392.
- 975 (17) (a) Huang, C.-Y.; Hsu, C.-Y.; Yang, L.-Y.; Lee, C.-J.; Yang, T.-F.; Hsu, C.-C.; Ke, C.-H.; Su, Y. O. A systematic study of electrochemical and spectral properties for the electronic interactions in porphyrin-triphenylamine conjugates. *Eur. J. Inorg. Chem.* **2012**, *2012*, 1038–1047. (b) Yao, C.-J.; Zhong, Y.-W.; Yao, J. Five-stage near-infrared electrochromism in electropolymerized films composed of alternating cyclometalated bisruthenium and bis-triarylamine segments. *Inorg. Chem.* **2013**, *52*, 10000–10008. (c) Lambert, C.; Nöll, G.; Schelter, J. Bridge-mediated hopping or superexchange electron-transfer processes in bis(triarylamine) systems. *Nat. Mater.* **2002**, *1*, 69–73. (d) Low, P. J.; Paterson, M. A.; Puschmann, H.; Goeta, A. E.; Howard, J. A.; Lambert, C.; Cherryman, J. C.; Tackley, D. R.; Leeming, S.; Brown, B. Crystal, Molecular and electronic structure of N,N' -diphenyl- N,N' -bis(2,4-dimethylphenyl)-1,1'-biphenyl-4, 4'-diamine and the corresponding radical cation. *Chem. - Eur. J.* **2004**, *10*, 83–91. (e) Barlow, S.; Risko, C.; Odom, S. A.; Zheng, S.; Coropceanu, V.; Beverina, L.; Brédas, J.-L.; Marder, S. R. Tuning delocalization in the radical cations of 1,4-bis[4-(diarylamino)styryl]benzenes, 2,5-bis[4-(diarylamino)styryl]thiophenes, and 2, 5-bis[4-(diarylamino)styryl]pyrroles through substituent effects. *J. Am. Chem. Soc.* **2012**, *134*, 10146–10155.
- 994 (18) (a) Grelaud, G.; Cador, O.; Roisnel, T.; Argouarch, G.; Cifuentes, M. P.; Humphrey, M. G.; Paul, F. Triphenylamine derivatives with para-disposed pendant electron-rich organoiron alkynyl substituents: defining the magnetic interactions in a trinuclear iron (III) trication. *Organometallics* **2012**, *31*, 1635–1642. (b) Cui, B.; Tang, J.-H.; Yao, J.-N.; Zhong, Y.-W. A molecular platform for multistate near-infrared electrochromism and flip-flop, flip-flap-flop, and ternary memory. *Angew. Chem., Int. Ed.* **2015**, *54*, 9192–9197.
- 1002 (c) Fink, D.; Weibert, B.; Winter, R. F. Redox-active tetra-ruthenium metallacycles: reversible release of up to eight electrons resulting in strong electrochromism. *Chem. Commun.* **2016**, *52*, 6103–6106. (d) Polit, W.; Exner, T.; Wuttke, E.; Winter, R. F. Vinylruthenium-triarylamine conjugates as electroswitchable polyelectrochromic NIR dyes. *BioInorg. React. Mech.* **2012**, *8*, 85–105. (e) Tang, J.-H.; Shao, J.-Y.; He, Y.-Q.; Wu, S.-H.; Yao, J.; Zhong, Y.-W. Transition from a metal-localized mixed-valence compound to a fully delocalized and bridge-biased electrophore in a ruthenium-amine-ruthenium trication system. *Chem. - Eur. J.* **2016**, *22*, 10341. (f) Cheng, H.-C.; Chiu, K. Y.; Lu, S. H.; Chen, C.-C.; Lee, Y. W.; Yang, T.-F.; Kuo, M. Y.; Chen, P. P. Y.; Su, Y. O. Linear oligoarylamines: electrochemical, EPR, and computational studies of their oxidative states. *J. Phys. Chem. A* **2015**, *119*, 1933–1942. (g) Onitsuka, K.; Ohara, N.; Takei, F.; Takahashi, S. Synthesis and redox properties of trinuclear ruthenium-acetylide complexes with tri(ethynylphenyl)amine bridge. *Dalton Trans.* **2006**, 3693–3698. (h) Grelaud, G.; Cifuentes, M. P.; Schwich, T.; Argouarch, G.; Petrie, S.; Stranger, R.; Paul, F.; Humphrey, M. G. Multistate redox-active metalated triarylamines. *Eur. J. Inorg. Chem.* **2012**, *2012*, 65–75. (i) Onitsuka, K.; Ohara, N.; Takei, F.; Takahashi, S. Organoruthenium dendrimers possessing tris(4-ethynylphenyl)-amine bridges. *Organometallics* **2008**, *27*, 25–27.
- 1024 (19) (a) Paul, F.; Lapinte, C. Organometallic molecular wires and other nanoscale-sized devices: an approach using the organoiron-(dppe)Cp*Fe building block. *Coord. Chem. Rev.* **1998**, *178–180*, 427–505. (b) Akita, M.; Tanaka, Y.; Naitoh, C.; Ozawa, T.; Hayashi, N.; Takeshita, M.; Inagaki, A.; Chung, M.-C. Synthesis of a series of diiron complexes based on a tetraethynylethene skeleton and related C_6 -enediynes spacers, (dppe)Cp*Fe–C≡CC(R)=C(R)C≡C–FeCp*-(dppe): tunable molecular wires. *Organometallics* **2006**, *25*, 5261–5275. (c) Tanaka, Y.; Inagaki, A.; Akita, M. A photoswitchable molecular wire with the dithienylethene (DTE) linker, (dppe)(η^5 -C₅Me₅)Fe–C≡C–DTE–C≡C–Fe(η^5 -C₅Me₅) (dppe). *Chem. Commun.* **2007**, 1169–1171. (d) Motoyama, K.; Koike, T.; Akita, M. Remarkable switching behavior of bimodally stimuli-responsive photochromic dithienylethenes with redox-active organometallic attachments. *Chem. Commun.* **2008**, 5812–5814. (e) Matsuura, Y.; Tanaka, Y.; Akita, M. *p*-Diethynylbenzene-based molecular wires, Fe–C≡C–*p*-C₆H₄–C≡C–Fe[Fe(η^5 -C₅Me₅) (dppe)]: Synthesis, substituent effects and unexpected formation of benzodifuran complex. *J. Organomet. Chem.* **2009**, *694*, 1840–1847. (f) Hatanaka, T.; Ohki, Y.; Kamachi, T.; Nakayama, T.; Yoshizawa, K.; Katada, M.; Tatsumi, K. Naphthalene and anthracene complexes sandwiched by two {(Cp*)-Fe^I} fragments: strong electronic coupling between the Fe^I centers. *Chem. - Asian J.* **2012**, *7*, 1231–1242. (g) Quardokus, R. C.; Lu, Y.; Wasio, N. A.; Lent, C. S.; Justaud, F.; Lapinte, C.; Kandel, S. A. Through-bond versus through-space coupling in mixed-valence molecules: observation of electron localization at the single-molecule scale. *J. Am. Chem. Soc.* **2012**, *134*, 1710–1714. (h) Ghazala, S. I.; Paul, F.; Toupet, L.; Roisnel, T.; Hapiot, P.; Lapinte, C. Di-organonon mixed valent complexes featuring “(η^5 -dppe)(η^5 -C₅Me₅)Fe” endgroups: smooth Class-III to Class-II transition induced by

- successive insertion of 1,4-phenylene units in a butadiyne-diyl bridge. *J. Am. Chem. Soc.* **2006**, *128*, 2463–2476.
- (20) Makhoul, R.; Sahnoune, H.; Dorcet, V.; Halet, J.-F.; Hamon, J.-R.; Lapinte, C. 1,2-diethynylbenzene-bridged $[\text{Cp}^*(\text{dppe})\text{Fe}]^{n+}$ units: effect of steric hindrance on the chemical and physical properties. *Organometallics* **2015**, *34*, 3314–3326.
- (21) (a) Fox, M. A.; Le Guennic, B.; Roberts, R. L.; Brue, D. A.; Yufit, D. S.; Howard, J. A. K.; Manca, G.; Halet, J.-F.; Hartl, F.; Low, P. J. Simultaneous bridge-localized and mixed-valence character in diruthenium radical cations featuring diethynylaromatic bridging ligands. *J. Am. Chem. Soc.* **2011**, *133*, 18433–18446. (b) Bruce, M. I.; Low, P. J.; Hartl, F.; Humphrey, P. A.; de Montigny, F.; Jevric, M.; Lapinte, C.; Perkins, G. J.; Roberts, R. L.; Skelton, B. W.; White, A. H. Syntheses, structures, some reactions, and electrochemical oxidation of ferrocenylethynyl complexes of iron, ruthenium, and osmium. *Organometallics* **2005**, *24*, S241–S255. (c) Bruce, M. I.; Burgun, A.; Fox, M. A.; Jevric, M.; Low, P. J.; Nicholson, B. K.; Parker, C. R.; Skelton, B. W.; White, A. H.; Zaitseva, N. N. Some ruthenium derivatives of penta-1, 4-diyn-3-one. *Organometallics* **2013**, *32*, 3286–3299. (d) Gao, L.-B.; Zhang, L.-Y.; Shi, L.-X.; Chen, Z.-N. Syntheses, characterization, redox properties, and mixed-valence chemistry of tetra- and hexanuclear diynyl complexes. *Organometallics* **2005**, *24*, 1678–1684.
- (22) (a) Bruce, M. I.; Hall, B. C.; Kelly, B. D.; Low, P. J.; Skelton, B. W.; White, A. H. An efficient synthesis of polyyne and polyyne-diyl complexes of ruthenium(II). *J. Chem. Soc., Dalton Trans.* **1999**, 3719–3728. (b) Bruce, M. I.; Ellis, B. G.; Gaudio, M.; Lapinte, C.; Melino, G.; Paul, F.; Skelton, B. W.; Smith, M. E.; Toupet, L.; White, A. H. Preparation, structures and some reactions of novel diynyl complexes of iron and ruthenium. *Dalton Trans.* **2004**, 1601–1609.
- (23) (a) Paul, F.; Ellis, B. G.; Bruce, M. I.; Toupet, L.; Roisnel, T.; Costuas, K.; Halet, J.-F.; Lapinte, C. Bonding and substituent effects in electron-rich mononuclear ruthenium σ -arylacetylides of the formula $[(\eta^2\text{-dppe})(\eta^5\text{-C}_5\text{Me}_5)\text{Ru}(\text{C}\equiv\text{C})\text{-1, 4-(C}_6\text{H}_4\text{X})][\text{PF}_6]_n$ ($n = 0, 1$; $\text{X} = \text{NO}_2, \text{CN}, \text{F}, \text{H}, \text{OMe}, \text{NH}_2$). *Organometallics* **2006**, *25*, 649–665. (b) Gendron, F.; Burgun, A.; Skelton, B. W.; White, A. H.; Roisnel, T.; Bruce, M. I.; Halet, J.-F.; Lapinte, C.; Costuas, K. Iron and ruthenium σ -polyyne of the general formula $[\{\text{M}(\text{dppe})\text{Cp}^*\}\text{-(C}\equiv\text{C)}_n\text{-R}]^{0/+}$ ($\text{M} = \text{Fe}, \text{Ru}$): an experimental and theoretical investigation. *Organometallics* **2012**, *31*, 6796–6811. (c) Bruce, M. I.; Costuas, K.; Davin, T.; Ellis, B. G.; Halet, J. F.; Lapinte, C.; Low, P. J.; Smith, M. E.; Skelton, B. W.; Toupet, L.; White, A. H. Iron versus Ruthenium: dramatic changes in electronic structure result from replacement of one Fe by Ru in $[\{\text{Cp}^*(\text{dppe})\text{Fe}\}\text{-C}\equiv\text{C-C}\equiv\text{C}\text{-}\{\text{Fe}(\text{dppe})\text{-Cp}^*\}]^{n+}$ ($n = 0, 1, 2$). *Organometallics* **2005**, *24*, 3864–3881. (d) Gauthier, N.; Argouarch, G.; Paul, F.; Toupet, L.; Ladjarafi, A.; Costuas, K.; Halet, J.-F.; Samoc, M.; Cifuentes, M. P.; Corkery, T. C.; Humphrey, M. G. Electron-rich iron/ruthenium arylalkynyl complexes for third-order nonlinear optics: redox-switching between three states. *Chem. - Eur. J.* **2011**, *17*, S561–S577. (e) Connelly, N. G.; Gamasa, M. P.; Gimeno, J.; Lapinte, C.; Lastra, E.; Maher, J. P.; Le Narvor, N.; Rieger, A. L.; Rieger, P. H. 17-Electron alkynyl complexes of cyclopentadienyliron(III). *J. Chem. Soc., Dalton Trans.* **1993**, 2575–2578. (f) Bruce, M. I.; Burgun, A.; Gendron, F.; Grelaud, G.; Halet, J.-F.; Skelton, B. W. Oxidative Dimerization of arylalkynyl–ruthenium complexes. *Organometallics* **2011**, *30*, 2861–2868. (g) Le Narvor, N.; Toupet, L.; Lapinte, C. Elemental carbon chain bridging two iron centers: syntheses and spectroscopic properties of $[\text{Cp}^*(\text{dppe})\text{Fe-C}_4\text{-FeCp}^*(\text{dppe})]^{n+} \bullet n[\text{PF}_6]^-$. X-ray crystal structure of the mixed valence complex ($n = 1$). *J. Am. Chem. Soc.* **1995**, *117*, 7129–7138. (h) Bruce, M. I.; Ellis, B. G.; Skelton, B. W.; White, A. H. Further reactions of some bis(vinylidene) diruthenium complexes. *J. Organomet. Chem.* **2005**, *690*, 792–801.
- (24) (a) Grelaud, G.; Cifuentes, M. P.; Schwich, T.; Argouarch, G.; Petrie, S.; Stranger, R.; Paul, F.; Humphrey, M. G. Multistate redox-active metalated triarylamines. *Eur. J. Inorg. Chem.* **2012**, *2012*, 65–75. (b) Polit, W.; Exner, T.; Wuttke, E.; Winter, R. F. Vinylruthenium-triarylamine conjugates as electroswitchable polyelectrochromic NIR dyes. *BioInorg. React. Mech.* **2012**, *8*, 85–105.
- (25) (a) Costuas, K.; Cador, O.; Justaud, F.; Le Stang, S.; Paul, F.; Monari, A.; Evangelisti, S.; Toupet, L.; Lapinte, C.; Halet, J.-F. 3, 5-Bis(ethynyl) pyridine and 2, 6-bis(ethynyl) pyridine spanning two $\text{Fe}(\text{Cp}^*)(\text{dppe})$ units: role of the nitrogen atom on the electronic and magnetic couplings. *Inorg. Chem.* **2011**, *50*, 12601–12622. (b) Parthey, M.; Gluyas, J. B. G.; Schauer, P. A.; Yufit, D. S.; Howard, J. A. K.; Kaupp, M.; Low, P. J. Refining the interpretation of near-infrared band shapes in a polyyne-diyl molecular wire. *Chem. - Eur. J.* **2013**, *19*, 9780–9784. (c) Parthey, M.; Kaupp, M. Quantum-chemical insights into mixed-valence systems: within and beyond the Robin–Day scheme. *Chem. Soc. Rev.* **2014**, *43*, 5067–5088. (d) Burgun, A.; Gendron, F.; Sumby, C.; Roisnel, T.; Cador, O.; Costuas, K.; Halet, J.-F.; Bruce, M. I.; Lapinte, C. Hexatriynediyl chain spanning two $\text{Cp}^*(\text{dppe})\text{M}$ termini ($\text{M} = \text{Fe}, \text{Ru}$): evidence for the dependence of electronic and magnetic couplings on the relative orientation of the termini. *Organometallics* **2014**, *33*, 2613–2627. (e) Makhoul, R.; Kumamoto, Y.; Miyazaki, A.; Justaud, F.; Gendron, F.; Halet, J.-F.; Hamon, J.-R.; Lapinte, C. Synthesis and properties of a mixed-valence compound with single-step tunneling and multiple-step hopping behavior. *Eur. J. Inorg. Chem.* **2014**, *2014*, 3899–3911. (f) Zhang, J.; Zhang, M.-X.; Sun, C.-F.; Xu, M.; Hartl, F.; Yin, J.; Yu, G.-A.; Rao, L.; Liu, S.-H. Diruthenium complexes with bridging diethynyl polyaromatic ligands: synthesis, spectroelectrochemistry, and theoretical calculations. *Organometallics* **2015**, *34*, 3967–3978. (g) Denis, R.; Toupet, L.; Paul, F.; Lapinte, C. Electron-rich piano-stool iron σ -acetylides bearing a functional aryl group. synthesis and characterization of iron (II) and iron (III) complexes. *Organometallics* **2000**, *19*, 4240–4251.
- (26) (a) Gauthier, N.; Tchouar, N.; Justaud, F.; Argouarch, G.; Cifuentes, M. P.; Toupet, L.; Touchard, D.; Halet, J.-F.; Rigaut, S.; Humphrey, M. G.; Costuas, K.; Paul, F. Bonding and electron delocalization in ruthenium (III) σ -arylacetylide radicals $[\text{trans-Cl}(\eta^2\text{-dppe})_2\text{RuC}\equiv\text{C}(4\text{-C}_6\text{H}_4\text{X})]^+$ ($\text{X} = \text{NO}_2, \text{C}(\text{O})\text{H}, \text{C}(\text{O})\text{Me}, \text{F}, \text{H}, \text{OMe}, \text{NMe}_2$): misleading aspects of the ESR anisotropy. *Organometallics* **2009**, *28*, 2253–2266. (b) Wuttke, E.; Pevny, F.; Hervault, Y.-M.; Norel, L.; Drescher, M.; Winter, R. F.; Rigaut, S. Fully delocalized (ethynyl) (vinyl) phenylene bridged triruthenium complexes in up to five different oxidation states. *Inorg. Chem.* **2012**, *51*, 1902–1915.
- (27) (a) Zhang, D.-B.; Wang, J.-Y.; Wen, H.-M.; Chen, Z.-N. Electrochemical, spectroscopic, and theoretical studies on diethynyl ligand bridged ruthenium complexes with 1, 3-bis(2-pyridylimino) isoindolate. *Organometallics* **2014**, *33*, 4738–4746. (b) Yao, C.-J.; Nie, H.-J.; Yang, W.-W.; Yao, J.; Zhong, Y.-W. Combined experimental and computational study of pyren-2,7-diyl-bridged diruthenium complexes with various terminal ligands. *Inorg. Chem.* **2015**, *54*, 4688–4698. (c) Fox, M. A.; Roberts, R. L.; Baines, T. E.; Le Guennic, B.; Halet, J.-F.; Hartl, F.; Yufit, D. S.; Albessa-Jové, D.; Howard, J. A. K.; Low, P. J. Ruthenium complexes of C,C'-bis(ethynyl) carboranes: an investigation of electronic interactions mediated by spherical pseudo-aromatic spacers. *J. Am. Chem. Soc.* **2008**, *130*, 3566–3578.
- (28) (a) Zhang, J.; Ou, Y.-P.; Xu, M.; Sun, C.-F.; Yin, J.; Yu, G.-A.; Liu, S. H. Synthesis and characterization of dibenzoheterocycle-bridged dinuclear ruthenium alkynyl and vinyl complexes. *Eur. J. Inorg. Chem.* **2014**, *2014*, 2941–2951. (b) Khairul, W. M.; Fox, M. A.; Schauer, P. A.; Yufit, D. S.; Albessa-Jové, D.; Howard, J. A. K.; Low, P. J. The electronic structures of diruthenium complexes containing an oligo(phenylene ethynylene) bridging ligand, and some related molecular structures. *Dalton Trans.* **2010**, *39*, 11605–11615. (c) Armit, D. J.; Bruce, M. I.; Gaudio, M.; Zaitseva, N. N.; Skelton, B. W.; White, A. H.; Le Guennic, B.; Halet, J.-F.; Fox, M. A.; Roberts, R. L.; Hartl, F.; Low, P. J. Some transition metal complexes derived from mono- and di-ethynyl perfluorobenzenes. *Dalton Trans.* **2008**, 6763–6775. (d) Klein, A.; Lavastre, O.; Fiedler, J. Role of the bridging arylethynyl ligand in Bi- and trinuclear ruthenium and iron complexes. *Organometallics* **2006**, *25*, 635–643.
- (29) Amthor, S.; Noller, B.; Lambert, C. UV/Vis/NIR spectral properties of triarylamines and their corresponding radical cations. *Chem. Phys.* **2005**, *316*, 141–152.
- (30) Weyland, T.; Ledoux, I.; Brasselet, S.; Zyss, J.; Lapinte, C. Nonlinear optical properties of redox-active mono-, bi-, and trimetallic

- 1193 σ -acetylide complexes connected through a phenyl ring in the
1194 $\text{Cp}^*(\text{dppe})\text{Fe}$ series. An example of electro-switchable NLO response.
1195 *Organometallics* **2000**, *19*, 5235–5237.
- 1196 (31) (a) Lambert, C.; Nöll, G. The class II/III transition in
1197 triarylamine redox systems. *J. Am. Chem. Soc.* **1999**, *121*, 8434–8442.
1198 (b) Cheng, H.-C.; Chiu, K. Y.; Lu, S. H.; Chen, C.-C.; Lee, Y. W.;
1199 Yang, T.-F.; Kuo, M. Y.; Chen, P. P.-Y.; Su, Y. O. Linear
1200 oligoarylamines: electrochemical, EPR, and computational studies of
1201 their oxidative states. *J. Phys. Chem. A* **2015**, *119*, 1933–1942.
- 1202 (32) (a) Parthey, M.; Gluyas, J. B. G.; Fox, M. A.; Low, P. J.; Kaupp,
1203 M. Mixed-valence ruthenium complexes rotating through a conforma-
1204 tional robin-day continuum. *Chem. - Eur. J.* **2014**, *20*, 6895–6908.
1205 (b) Marqués-González, S.; Parthey, M.; Yufit, D. S.; Howard, J. A. K.;
1206 Kaupp, M.; Low, P. J. Combined spectroscopic and quantum chemical
1207 study of $[\text{trans-Ru}(\text{C}\equiv\text{CC}_6\text{H}_4\text{R}^1\text{-4})_2(\text{dppe})_2]^{n+}$ and $[\text{trans-Ru}(\text{C}\equiv\text{CC}_6\text{H}_4\text{R}^1\text{-4})(\text{C}\equiv\text{CC}_6\text{H}_4\text{R}^2\text{-4})(\text{dppe})_2]^{n+}$ ($n = 0, 1$) complexes:
1208 interpretations beyond the lowest energy conformer paradigm.
1209 *Organometallics* **2014**, *33*, 4947–4963.
- 1210 (33) (a) Hush, N. S. Intervalence-transfer absorption. Part 2.
1211 Theoretical considerations and spectroscopic data. *Prog. Inorg. Chem.*
1212 **1967**, *8*, 391–444. (b) Hush, N. S. Distance dependence of electron
1213 transfer rates. *Coord. Chem. Rev.* **1985**, *64*, 135–157. (c) Hush, N. S.
1214 Homogeneous and heterogeneous optical and thermal electron
1215 transfer. *Electrochim. Acta* **1968**, *13*, 1005–1023.
- 1216 (34) (a) Hamon, P.; Justaud, F.; Cadot, O.; Hapiot, P.; Rigaut, S.;
1217 Toupet, L.; Ouahab, L.; Stueger, H.; Hamon, J.-R.; Lapinte, C. Redox-
1218 active organometallics: magnetic and electronic couplings through
1219 carbon-silicon hybrid molecular connectors. *J. Am. Chem. Soc.* **2008**,
1220 *130*, 17372–17383. (b) Paul, F.; Toupet, L.; Thépot, J.-Y.; Costuas,
1221 K.; Halet, J.-F.; Lapinte, C. Electron-rich piano-stool iron σ -acetylides.
1222 Electronic structures of arylalkynyl iron (III) radical cations.
1223 *Organometallics* **2005**, *24*, 5464–5478.
- 1224 (35) Shi, L. Q.; He, C.; Zhu, D. F.; He, Q. G.; Li, Y.; Chen, Y.; Sun,
1225 Y. X.; Fu, Y. Y.; Wen, D.; Cao, H. M.; Cheng, J. G. High performance
1226 aniline vapor detection based on multi-branched fluorescent triphenyl-
1227 amine-benzothiadiazole derivatives: branch effect and aggregation
1228 control of the sensing performance. *J. Mater. Chem.* **2012**, *22*, 11629–
1229 11635.
- 1230 (36) Sirohi, R.; Kim, D. H.; Yu, S.-C.; Lee, S. H. Novel di-anchoring
1231 dye for DSSC by bridging of two mono anchoring dye molecules: a
1232 conformational approach to reduce aggregation. *Dyes Pigm.* **2012**, *92*,
1233 1132–1137.
- 1234 (37) Bruce, M. I.; Ellis, B. G.; Low, P. J.; Skelton, B. W.; White, A. H.
1235 Syntheses, structures, and spectro-electrochemistry of $\{\text{Cp}^*(\text{PP})\text{Ru}\}$ -
1236 $\text{C}\equiv\text{CC}\equiv\text{C}\{\text{Ru}(\text{PP})\text{Cp}^*\}$ ($\text{PP} = \text{dppm}, \text{dppe}$) and their mono-and
1237 dications. *Organometallics* **2003**, *22*, 3184–3198.
- 1238 (38) Roger, C.; Hamon, P.; Toupet, L.; Rabaâ, H.; Saillard, J.-Y.;
1239 Hamon, J.-R.; Lapinte, C. Alkyl (pentamethylcyclopentadienyl)(1, 2-
1240 bis (diphenylphosphino)-ethane) iron (III) 17-electron complexes:
1241 synthesis, NMR and magnetic properties, and EHMO calculations.
1242 *Organometallics* **1991**, *10*, 1045–1054.
- 1243 (39) Fang, Z.; Samoc, M.; Webster, R. D.; Samoc, A.; Lai, Y. H.
1244 Triphenylamine derivatized phenylacetylene macrocycle with large
1245 two-photon absorption cross-section. *Tetrahedron Lett.* **2012**, *53*,
1246 4885–4888.
- 1247 (40) Sheldrick, G. M. *SHELXS-97, a Program for Crystal Structure*
1248 *Solution*; University of Göttingen: Göttingen, Germany, 1997.
- 1249 (41) Sheldrick, G. M. *SHELXL-97, a Program for Crystal Structure*
1250 *Refinement*; University of Göttingen, Göttingen, Germany, 1997.
- 1251 (42) Krejčík, M.; Daněk, M.; Hartl, F. Simple construction of an
1252 infrared optically transparent thin-layer electrochemical cell: Applica-
1253 tions to the redox reactions of ferrocene, $\text{Mn}_2(\text{CO})_{10}$ and $\text{Mn}(\text{CO})_3$
1254 $(3,5\text{-di-}t\text{-butyl-catecholate})^-$. *J. Electroanal. Chem. Interfacial Electro-*
1255 *chem.* **1991**, *317*, 179–187.
- 1256 (43) Frisch, M. J.; Trucks, G. W.; Schlegel, H. B.; Scuseria, G. E.;
1257 Robb, M. A.; Cheeseman, J. R.; Scalmani, G.; Barone, V.; Mennucci,
1258 B.; Petersson, G. A.; Nakatsuji, H.; Caricato, M.; Li, X.; Hratchian, H.
1259 P.; Izmaylov, A. F.; Bloino, J.; Zheng, G.; Sonnenberg, J. L.; Hada, M.;
1260 Ehara, M.; Toyota, K.; Fukuda, R.; Hasegawa, J.; Ishida, M.; Nakajima,
1261 T.; Honda, Y.; Kitao, O.; Nakai, H.; Vreven, T.; Montgomery, J. A., Jr.;
1262 Peralta, J. E.; Ogliaro, F.; Bearpark, M.; Heyd, J. J.; Brothers, E.; Kudin,
1263 K. N.; Staroverov, V. N.; Kobayashi, R.; Normand, J.; Raghavachari, K.;
1264 Rendell, A.; Burant, J. C.; Iyengar, S. S.; Tomasi, J.; Cossi, M.; Rega,
1265 N.; Millam, J. M.; Klene, M.; Knox, J. E.; Cross, J. B.; Bakken, V.;
1266 Adamo, C.; Jaramillo, J.; Gomperts, R.; Stratmann, R. E.; Yazyev, O.;
1267 Austin, A. J.; Cammi, R.; Pomelli, C.; Ochterski, J. W.; Martin, R. L.;
1268 Morokuma, K.; Zakrzewski, V. G.; Voth, G. A.; Salvador, P.;
1269 Dannenberg, J. J.; Dapprich, S.; Daniels, A. D.; Farkas, Ö.;
1270 Foresman, J. B.; Ortiz, J. V.; Cioslowski, J.; Fox, D. J. *Gaussian 09*,
1271 Revision D.01; Gaussian, Inc.: Wallingford, CT, 2009.
- 1272 (44) Renz, M.; Theilacker, K.; Lambert, C.; Kaupp, M. A reliable
1273 quantum-chemical protocol for the characterization of organic mixed-
1274 valence compounds. *J. Am. Chem. Soc.* **2009**, *131*, 16292–16302.
- 1275 (45) (a) Cossi, M.; Rega, N.; Scalmani, G.; Barone, V. Energies,
1276 structures, and electronic properties of molecules in solution with the
1277 C-PCM solvation model. *J. Comput. Chem.* **2003**, *24*, 669–681.
- 1278 (b) Barone, V.; Cossi, M. Quantum calculation of molecular energies
1279 and energy gradients in solution by a conductor solvent model. *J. Phys.*
1280 *Chem. A* **1998**, *102*, 1995–2001.
- 1281